RESEARCH ARTICLE

WILEY

Pilotins are mobile T3SS components involved in assembly and substrate specificity of the bacterial type III secretion system

Stephan Wimmi[1] | Moritz Fleck[1] | Carlos Helbig[1] | Corentin Brianceau[1] | Katja Langenfeld[1] | Witold G. Szymanski[2] | Georgia Angelidou[2] | Timo Glatter[2] | Andreas Diepold ⓘ[1]

[1]Department of Ecophysiology, Max Planck Institute for Terrestrial Microbiology, Marburg, Germany

[2]Mass Spectrometry and Proteomics Facility, Max Planck Institute for Terrestrial Microbiology, Marburg, Germany

Correspondence
Andreas Diepold, Department of Ecophysiology, Max Planck Institute for Terrestrial Microbiology, Karl-von-Frisch-Str. 10, 35043 Marburg, Germany.
Email: andreas.diepold@mpi-marburg.mpg.de
Witold G. Szymanski, Department of Medicine, Institute of Translational Proteomics, Phillips University Marburg, Marburg, Germany

Present address
Stephan Wimmi, Institute for Biological Physics, University of Cologne, Köln, Germany

Funding information
Max-Planck-Gesellschaft

Abstract

In animal pathogens, assembly of the type III secretion system injectisome requires the presence of so-called pilotins, small lipoproteins that assist the formation of the secretin ring in the outer membrane. Using a combination of functional assays, interaction studies, proteomics, and live-cell microscopy, we determined the contribution of the pilotin to the assembly, function, and substrate selectivity of the T3SS and identified potential new downstream roles of pilotin proteins. In absence of its pilotin SctG, *Yersinia enterocolitica* forms few, largely polar injectisome sorting platforms and needles. Accordingly, most export apparatus subcomplexes are mobile in these strains, suggesting the absence of fully assembled injectisomes. Remarkably, while absence of the pilotin all but prevents export of early T3SS substrates, such as the needle subunits, it has little effect on secretion of late T3SS substrates, including the virulence effectors. We found that although pilotins interact with other injectisome components such as the secretin in the outer membrane, they mostly localize in transient mobile clusters in the bacterial membrane. Together, these findings provide a new view on the role of pilotins in the assembly and function of type III secretion injectisomes.

KEYWORDS
bacterial virulence mechanisms, host pathogen interaction, live cell microscopy, membrane transport, secretion systems

1 | INTRODUCTION

Bacteria that live in contact with eukaryotic cells greatly benefit from being able to manipulate those cells. The bacterial type III secretion system (T3SS) allows such manipulation by injecting effector proteins directly from the bacterial cytosol into the host cell cytoplasm (Burkinshaw & Strynadka, 2014; Büttner, 2012; Cornelis, 2006; Galán & Wolf-Watz, 2006; Wagner et al., 2018). Although the T3SS is also used by symbionts and commensals (Coombes, 2009; Miwa & Okazaki, 2017), it is best known for its essential role in infections of

important human pathogens such as *Salmonella*, *Shigella*, and *Yersinia*. In these pathogens, the T3SS machinery, also called injectisome,[1] is often assembled upon entry into the host organism. Once the basal body (membrane rings and export apparatus, Figure 1a) and the cytosolic components are assembled (reviewed in Diepold & Wagner, 2014), the T3SS starts to secrete its own distal components. Among those so-called early secretion substrates are the subunits of the needle and proteins required for its correct assembly, as well as early regulatory proteins. When the required needle length is reached (Journet et al., 2003; Wee & Hughes, 2015), middle secretion substrates—the translocon proteins forming the needle tip and two hydrophobic interactors that build a pore in the host membrane—are secreted. At this point, the injectisome is ready for secretion of the late secretion substrates, the virulence effectors, which is initiated by host cell contact.

Injectisomes are assembled at the bacterial surface according to the needs of the bacteria in a given situation. While in some cases, one to few injectisomes are sufficient (such as for the intracellular *Salmonella* SPI-2 T3SS (Chakravortty et al., 2005)), bacteria that need to actively make contact with the host cells usually build more injectisomes (Blocker et al., 1999; Diepold & Armitage, 2015). In many species, injectisomes are distributed across the bacterial surface (Burgess et al., 2020; Diepold et al., 2010; Zhang et al., 2017). Statistical analysis in *Y. enterocolitica* suggested a non-random localization (Kudryashev et al., 2015), but it is currently unclear what determines where new injectisomes are built.

A prime candidate to establish the sites of assembly for new injectisomes is the pilotin, a lipoprotein anchored in the inner leaflet of the outer membrane (OM). Pilotins are required for the proper integration and oligomerization of the secretin protein, which forms a large channel in the OM in the T3SS of animal pathogens, but also type II secretion systems (T2SS) and type IV pili (T4P) (Allaoui et al., 1995; Burghout et al., 2004; Gu et al., 2012; Hardie et al., 1996; Koo et al., 2012; Korotkov et al., 2011; Nouwen et al., 1999; Perdu et al., 2015; Rau & Darwin, 2015; Schuch & Maurelli, 2001; Silva et al., 2020). Since the secretin ring is one of the nucleation structures of the injectisome (Diepold et al., 2010; Diepold & Wagner, 2014) and anchors the T3SS at its final position in the peptidoglycan mesh (Diepold et al., 2011) (Figure 1a), the localization of the pilotin may determine the place of secretin ring formation and in consequence the distribution of injectisomes.

Pilotins and their cognate secretin proteins in the T2SS and T3SS have been purified and structurally analyzed in 1:1 complexes (Majewski et al., 2021; Nouwen et al., 1999; Okon et al., 2008). As a lipoprotein, the pilotin also interacts with the localization of lipoproteins (Lol) protein export machinery (Collin et al., 2011; Majewski et al., 2021). Based on these properties, different models for the export of the pilotin itself and its role in secretin ring assembly have been proposed (Majewski et al., 2021; Okon et al., 2008). Whether

the pilotin stays attached to the secretin after secretin ring formation in the OM and the subsequent assembly of the injectisome is debated and might differ between organisms. For T2SS secretins, such attachment was initially proposed, but later rejected (Chami et al., 2005; Nouwen et al., 1999); recent analyses of purified secretin rings found pilotins attached stoichiometrically outside the main ring (Chernyatina & Low, 2019; Yin et al., 2018). In situ structures of the T3SS showed electron densities around the secretin, possibly corresponding to pilotin proteins, in *Shigella flexneri* (Flacht et al., 2023; Hu et al., 2015), but not in *Salmonella enterica* (Hu et al., 2017, 2018; Miletic et al., 2021). In spite of the importance of pilotins for the nucleation and localization of the central secretin ring structure (which also prevents ion leakage caused by secretin misassembly in the inner membrane (Burghout et al., 2004; Collin et al., 2011; Majewski et al., 2021)), protein secretion by the T3SS was found to be strongly impaired, but not completely prevented in absence of the pilotin in different organisms (Allaoui et al., 1995; Burghout et al., 2004; Perdu et al., 2015). Likewise, the number of needles formed was strongly reduced in a pilotin mutant in *P. aeruginosa* (Perdu et al., 2015). The impact on secretion varied between different bacteria and substrates, and the reason for this phenotype is currently unclear. Pilotins have a conserved unique genetic location within the virulence plasmids or genetic islands encoding the T3SS. While most other structural and regulatory components of the injectisome are encoded in operons under the control of a main transcriptional regulator (VirF in *Y. enterocolitica*, called LcrF in other *Yersinia* species), pilotins are located upstream of the transcriptional regulator itself, indicating a specific role in the T3SS with a potentially distinct expression pattern.

Despite their central role, many key characteristics of pilotins are poorly understood or debated: Why are pilotins encoded differently from all other T3SS components? When and where are they active and does this determine the assembly and localization of injectisomes? Do pilotins remain part of the injectisome after the assembly and do they adopt a functional role in type III secretion at this point?

To shed light on these questions and the role of pilotins in assembly and function of the T3SS, we studied the role of the *Yersinia enterocolitica* pilotin SctG[2] with functional assays, fluorescence microscopy, proteomics, as well as protein interaction and dynamics studies. While we confirmed the known interaction of SctG with the secretin SctC, the majority of fluorescently labeled SctG localized in dynamic patches that are dispersed throughout the bacterial membrane. In absence of the pilotin, only a small subset of bacteria assemble single, mostly polar needles which are not stably attached to fully assembled injectisomes. Most notably, presence of the pilotin not only influenced injectisome assembly and overall secretion levels but specifically altered the secretion pattern of the T3SS. While effector proteins and other late substrates were efficiently secreted in the absence of the pilotin, the export of early substrates, such as

---

[1]The T3SS is at the core of both injectisomes and bacterial flagella (Diepold & Armitage, 2015; Erhardt et al., 2010). In this manuscript, "T3SS" refers to the injectisome-type, virulence-associated system.

[2]This manuscript uses the common nomenclature for T3SS components (Hueck, 1998; Wagner & Diepold, 2020); the species-specific nomenclature of the *Yersinia* pilotin is YscW; other names can be found in Table S1.

the needle components, was greatly impaired. Based on specific interaction studies, we provide possible explanations for this unique phenotype and an extended model for the function of the pilotin.

2 | RESULTS

2.1 | Deletion of the pilotin specifically reduces secretion of early export substrates

To define the overall role of the pilotin SctG in type III secretion, we tested the effects of a complete deletion of the *sctG* gene on the virulence plasmid in *Y. enterocolitica* (Figure S1). We found that absence of SctG distinctly altered the secretion pattern. While secretion of effector proteins was reduced, but still clearly present, early secretion substrates such as the needle subunit SctF, the ruler protein SctP, and translocators SctA, B, E were much more severely affected in secretion or not secreted at all. *In trans* expression of SctG complemented the deletion (Figures 1b and S2a).

In order to determine the role of SctG in secretion more precisely, we analyzed the secretome of the wild-type and Δ*sctG* strains by label-free quantitative mass spectrometry. The results confirm the secretion assay and show that T3SS substrates cluster according to their substrate class, rather than their overall secretion level (Figures 1c and S2b; Table 1): The late substrates, effector proteins YopH, O, P, E, M, T as well as the gatekeeper SctW (YopN) and the negative regulators YscM1/2 (marked green in Figure 1b,c,d), were exported remarkably efficiently in absence of SctG. In clear contrast, export of all early and middle substrates of the T3SS (marked magenta in Figure 1b,c,d) was strongly reduced in Δ*sctG*. These T3SS substrates build up the needle (SctF) and the inner rod (SctI) connecting it to the export apparatus, control needle length (SctP) and form its tip structure (SctA) as well as a pore in the host membrane (SctB, E). YscX is an early T3SS substrate specific to the Ysc subgroup of T3SS (Abby & Rocha, 2012; Troisfontaines & Cornelis, 2005), which is required for the export of any protein by Ysc subgroup of injectisomes (Diepold et al., 2012; Iriarte & Cornelis, 1999). Notably, no significant contribution of cell lysis was detectable, and secretion of the late substrates is fully T3SS-dependent, as no secretion was observed in a Δ*sctD* strain (Figure 1b) or under non-secreting conditions (Figure S2c), excluding export via alternative routes such as the flagellar T3SS. The specific reduction of secretion of
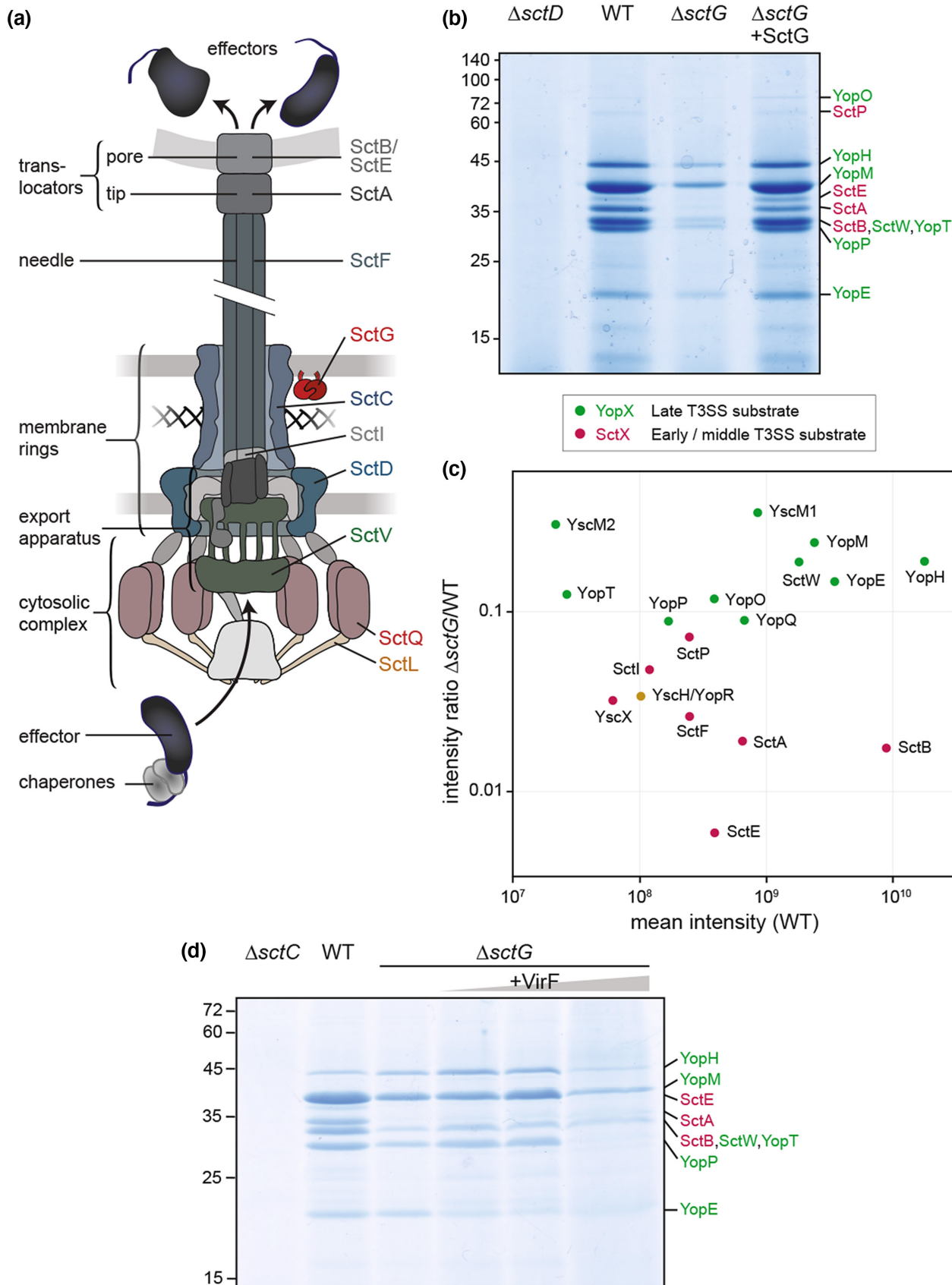
early export substrates in absence of the pilotin was confirmed by immunoblot analysis against the early substrates SctA, SctF, and YscX, as well as the complementary secretion pattern of the Δ*sctG* and a strain lacking the main virulence effectors YopH,O,P,E,M,T (Figure S3a,b). In supplemented microscopy medium, a minimal medium which allows for a more quantitative analysis by proteomics approaches, overall secretion levels were reduced, but an even more pronounced selective export of late substrates could be observed (Table 1, Figure S2a,b).

Most pilotins, including SctG, are expressed in an operon with the main transcription factor of the T3SS, VirF, which is encoded downstream of *sctG* in the same operon and whose expression is controlled by an RNA thermometer structure located between the two genes (Böhme et al., 2012; Schwiesow et al., 2016). We therefore tested the influence of a *sctG* deletion on VirF expression levels. In Δ*sctG*, the amount of the main transcriptional activator VirF was reduced to about one-third. Consequently, most other T3SS components were also present at lower concentrations (Table S2). In an effort to circumvent the reduction in VirF expression caused by the full deletion of *sctG*, we replaced Met-32 of *sctG* with a stop codon (see Figure S1). Surprisingly, this introduction further decreased VirF levels and, accordingly, overall secretion levels in *sctG*$_{stop}$ (Table S3, Figure S4). To test if the observed specific reduction in secretion of early substrates was caused by this impaired VirF expression in the absence of *sctG*, we therefore expressed VirF from plasmid in Δ*sctG* and *sctG*$_{stop}$. Indeed, this slightly increased the secretion of effectors, but not of early substrates (Figures 1d and S4), indicating that the specific loss of secretion of these early substrates is not caused by altered VirF expression in absence of *sctG*. These results highlight that the selective export observed in the absence of the pilotin (Figure 1b,c, Table 1) is retained upon complementation of the reduced VirF levels (Table S4) and is not due to differential expression of the respective export cargo (Table S2).

2.2 | The pilotin is essential for stable localization of the export apparatus and the cytosolic T3SS components, but few needles can form in its absence

We next investigated the specific role of the pilotin in the assembly of the injectisome, which may provide a clue to its specific impact on

FIGURE 1 SctG is required for the secretion of early export substrates, but not of effectors. (a) Schematic illustration of the injectisome (adapted from Diepold & Wagner, 2014). Main substructures indicated on the left; components analyzed in this study, including the pilotin SctG (for which a possible location is indicated, see main text) and the secretin SctC, are indicated on the right and shown in color. (b) Secretion assay showing the export of native T3SS substrates into the culture supernatant in the listed strains in rich medium ($n=3$). Normalized amounts of supernatant (equivalent to 3×10^8 bacteria per lane) were loaded on a SDS-PAGE gel and stained with Coomassie Brilliant Blue. Left, molecular weight in kDa; right, assignment of exported proteins. (c) Label-free mass spectrometry quantification of secreted proteins in Δ*sctG* and wild-type (WT) in rich medium, intensity ratio (Δ*sctG*/WT) plotted against mean intensity ($n=3$). See Figure S2 for comparison between rich and supplemented microscopy medium. (d) Secretion assay in rich medium for the indicated strains. Left, molecular weight in kDa. VirF expression from plasmid was induced with IPTG concentrations of 0, 10, 200μM (from left to right). Overexpression of VirF by induction with 200μM IPTG consistently decreased secretion and led to cell lysis, resulting in lower bacterial densities ($OD_{600}=3.1\pm0.6$, 3.0 ± 0.6, 1.1 ± 0.1 for 0, 10, 200μM IPTG, respectively) and a widening of the respective lane on the gel. Left, molecular weight in kDa; right, assignment of exported proteins. $n=3$. In all panels, early/middle T3SS export substrates are marked in magenta; late substrates (effectors) are marked in green; substrate with unknown time point of export marked in yellow.

(a)

(b) ΔsctD   WT   ΔsctG   ΔsctG +SctG

(c)

● YopX   Late T3SS substrate
● SctX   Early / middle T3SS substrate

(d) ΔsctC   WT   ΔsctG   +VirF

secretion specificity. To this aim, we deleted *sctG* in strains expressing fluorescently labeled variants of the secretin (SctC-mCherry) (Diepold et al., 2010), the large export apparatus component (SctV-EGFP)

(Diepold et al., 2011), the cytosolic sorting platform component SctL (mCherry-SctL) (Diepold et al., 2017), and a strain expressing SctF$_{S5C}$, a needle protein variant that can be labeled by maleimide dyes

TABLE 1 Influence of SctG on T3SS secretion substrates.

Rich medium T3SS substrate	# pept.	Intensity ratio ΔsctG/WT	Mean intensity WT	ΔsctG	ΔsctD
Translocator SctE (YopB)	29	0.0059	3.89E+08	2.29E+06	3.27E+05
Translocator SctB (YopD)	73	0.0174	8.87E+09	1.54E+08	2.76E+06
Tip protein SctA (LcrV)	41	0.0190	6.48E+08	1.23E+07	7.97E+04
Needle component SctF	8	0.0261	2.47E+08	6.45E+06	1.61E+05
Early substrate / regulator YscX	9	0.0321	6.09E+07	1.95E+06	3.06E+05
Secreted protein YscH/YopR	8	0.0339	1.01E+08	3.43E+06	5.17E+04
Rod / washer protein SctI	8	0.0476	1.19E+08	5.66E+06	5.20E+04
Needle length regul. / ruler SctP	33	0.0724	2.46E+08	1.78E+07	7.78E+05
Effector YopP	41	0.0886	1.68E+08	1.49E+07	7.50E+04
Effector YopQ	24	0.0895	6.70E+08	6.00E+07	8.07E+05
Effector YopO	71	0.1178	3.87E+08	4.55E+07	1.21E+05
Effector YopT	13	0.1246	2.64E+07	3.29E+06	4.27E+04
Effector YopE	25	0.1473	3.47E+09	5.10E+08	7.83E+05
Gatekeeper SctW (YopN)	19	0.1890	1.81E+09	3.42E+08	1.06E+06
Effector YopH	122	0.1906	1.78E+10	3.39E+09	3.17E+06
Effector YopM	8	0.2428	2.39E+09	5.81E+08	1.46E+06
Regulator YscM2	9	0.3061	2.16E+07	6.61E+06	5.69E+04
Regulator YscM1	21	0.3562	8.54E+08	3.04E+08	7.61E+05

| *Suppl. microscopy medium* T3SS substrate	# pept.	Intensity ratio ΔsctG/WT	Mean intensity WT	ΔsctG	ΔsctC
Needle component SctF	7	0.0547	3.95E+09	2.16E+08	1.65E+07
Early substrate / regulator YscX	4	0.1366	3.55E+08	4.85E+07	8.80E+06
Tip protein SctA (LcrV)	24	0.1580	8.72E+09	1.38E+09	1.07E+08
Rod / washer protein SctI	3	0.1621	3.56E+08	5.78E+07	2.07E+07
Needle length regul. / ruler SctP	23	0.2359	1.53E+09	3.60E+08	4.84E+07
Translocator SctE (YopB)	19	0.3213	2.73E+09	8.77E+08	3.44E+08
Translocator SctB (YopD)	46	0.4502	3.26E+10	1.47E+10	9.06E+08
Secreted protein YscH/YopR	4	0.5604	2.90E+08	1.62E+08	1.15E+07
Effector YopQ	16	0.6357	1.90E+09	1.21E+09	6.51E+06
Effector YopO	37	0.9833	1.72E+09	1.69E+09	6.58E+07
Effector YopH	64	1.1095	3.11E+10	3.45E+10	1.23E+09
Effector YopE	10	1.5746	1.16E+10	1.82E+10	2.67E+09
Effector YopP	25	2.1810	7.21E+08	1.57E+09	5.24E+06
Gatekeeper SctW (YopN)	17	2.5811	3.65E+09	9.42E+09	3.18E+07
Effector YopM	6	2.6303	4.81E+09	1.26E+10	7.99E+07
Effector YopT	7	4.1605	1.15E+07	4.77E+07	1.28E+07
Regulator YscM1	12	5.5968	4.84E+08	2.71E+09	9.81E+06
Regulator YscM2	7	10.2833	4.52E+07	4.65E+08	5.43E+06

Note: Label-free quantitative mass spectrometry of known T3SS substrates in the culture supernatant of different strains, as indicated. Top, measurement in rich medium; bottom, in supplemented microscopy medium (see material and methods for details). Magenta shade, early and middle substrates; green shade, late substrates; yellow shade, unknown. # pept., number of total detected peptides. Light gray font, imputed values (no peptides detected in at least one sample). Hits sorted by ratio of ΔsctG/wild-type (WT). n=3, individual measurements listed in Table S5.

(Milne-Davies et al., 2019). Except for SctF$_{S5C}$, which is expressed from a plasmid, all other labeled proteins are expressed from their native genetic environment. As expected, fluorescence microscopy of the respective bacteria showed an important role of SctG in the assembly of the secretin ring. Far from its usual assembly in >10 mostly lateral foci in the wild-type background, SctC mostly localized in large, often polar clusters in the absence of the pilotin (in 89.6% of bacteria, Figure 2a, left, Dataset S1). We found that these SctC foci generally do not correspond to fully assembled injectisomes: The cytosolic component SctL formed very few foci in the absence of SctG (in 6.6% of bacteria, Figure 2, center; Dataset S1), and SctV foci were mobile in the membrane in the absence of SctG, similar to their previously characterized behavior in the absence of the secretin SctC (Figures 2b and S5a) (Diepold et al., 2011). Nevertheless, a small subset of bacteria lacking SctG did display needles (4.6% of bacteria, Figure 2a, right; Dataset S1). These needles, however, did not

FIGURE 2 SctG is required for normal localization of SctC and stable assembly of the export apparatus and the sorting platform component SctL, but not fully essential for the formation of needles. (a) Fluorescence micrographs of *Y. enterocolitica* expressing the proteins indicated from their native location on the virulence plasmid (SctC-mCherry and mCherry-SctL) or *in trans* (SctF$_{S5C}$, stained with CF 488A maleimide stain) under secreting conditions in an effector-less strain background. Top row displays native localization in wild-type (WT) background, bottom row localization in respective Δ*sctG* strain background. Scale bar, 2 μm. The fraction of bacteria with foci is listed for the respective Δ*sctG* strains. See Dataset S1 for details. *n* = 3–6. (b) Red/green/blue (RGB) overlay and minimum intensity projection showing the movement of SctV-EGFP over time in the indicated effector-less strain backgrounds in live *Y. enterocolitica*. Red/green/blue channel: micrograph at *t* = 0/15/30 s; white foci indicate stable protein localization, whereas colors indicate movement of foci over time. Minimum projection of micrographs at 0/15/30/45/60/75/90 s; foci indicate stable foci over this time period. Numbers represent the average number of detected stable foci per bacterium. Bottom, graphic representation of stable and motile foci, corresponding to the images above. *n* = 3.
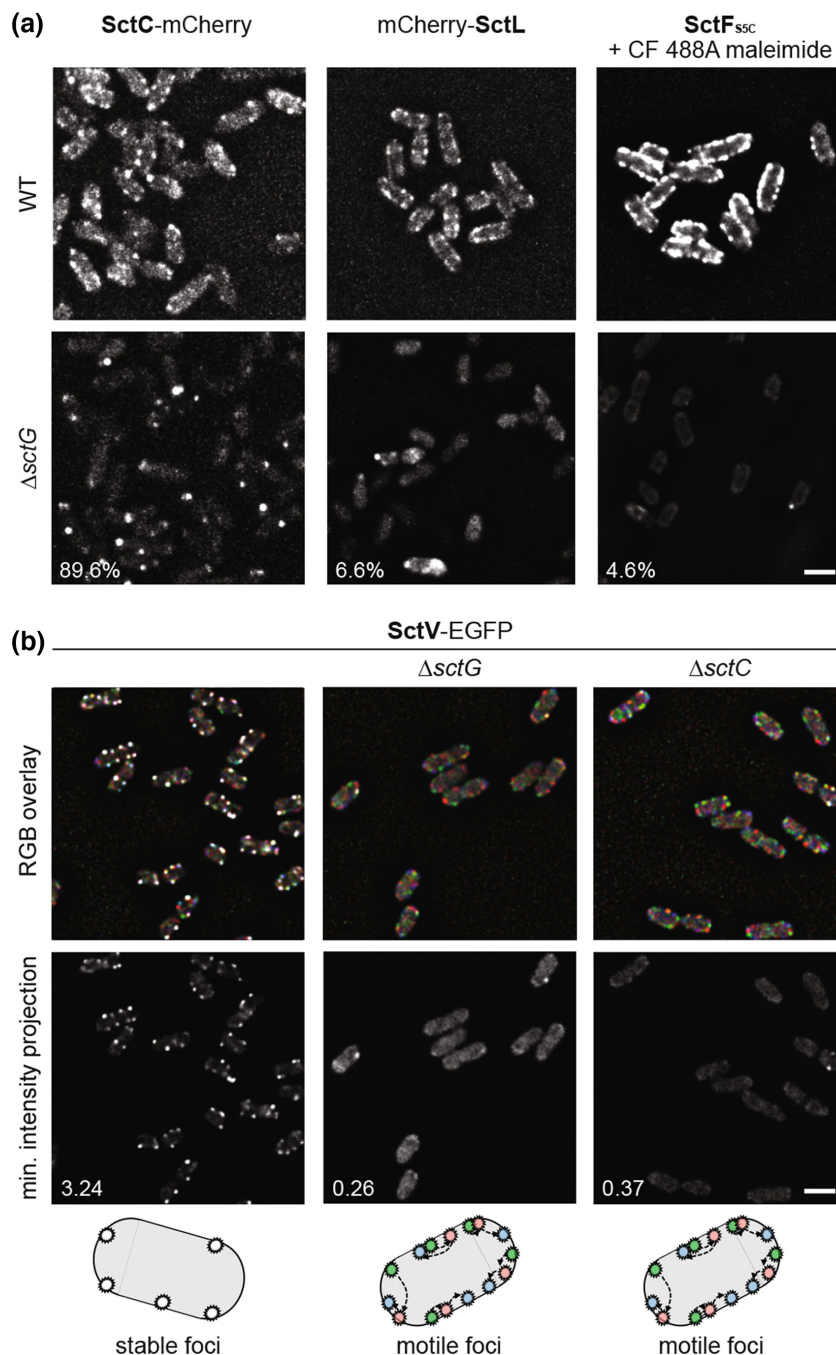
colocalize with the sorting platform protein SctL (Figure S5b). *In trans* complementation of SctG restored wild-type localization of all tested components (Figure S6). Notably, levels of SctG significantly lower than in the wild-type were already sufficient for complementation of secretion and injectisome assembly (Figure S6a–c).

The results above confirm previous findings that SctG, most likely through promoting the assembly of SctC in the OM, is essential for proper assembly and anchoring of all major subcomplexes of the injectisome. Strikingly, however, a subset of cells form mostly polar needles in its absence. We therefore took a closer look at the interactions, expression kinetics, and localization of SctG, to figure out how it conveys its function.

2.3 | Proteome analysis and specific interactions of the pilotin to T3SS components and proteins not directly linked to the T3SS

The finding that SctG amounts below the wild-type level are sufficient for its function in injectisome assembly (Figure S6) prompted us to consider additional roles of the pilotin. To identify such roles in an unbiased way, we compared the full *Y. enterocolitica* proteome in presence and absence of SctG under non-secreting conditions. Absence of SctG had little impact beyond the T3SS, with the notable exception of the OM protein OmpW, whose amount was reduced by a factor of eight (Table S2).

To unravel the expression kinetics, as well as the subcellular localization of SctG, we introduced a *sctG-sfGFP* fusion in the native *sctG* locus on the *Y. enterocolitica* virulence plasmid by homologous recombination (Kaniga et al., 1991). The SctG-sfGFP fusion protein was stable and functional (Figure S7). The expression of SctG itself, VirF, and, in consequence, other T3SS components was moderately increased (1.5–2-fold) in the strain; additionally, few non-T3SS proteins were affected by the fusions (Table S6).

In an attempt to better understand the function of the pilotin, both with respect to the T3SS and other pathways, we then screened for interaction partners by co-immunoprecipitation with SctG-sfGFP, analyzed by label-free mass spectrometry. Confirming the specificity of the co-immunoprecipitation experiment, SctG interacted with the secretin SctC, but also with other T3SS components, most prominently the effector YopM and the large export apparatus protein SctV (Figure 3). Most other T3SS components were enriched to a lower degree (Figure 3, Table S7).

Interestingly, a number of proteins not directly linked to the T3SS were enriched highly significantly. Most prominently, the phosphoenolpyruvate (PEP)-dependent phosphotransferase system (PTS) trehalose transporter subunit EIIBC (PTS-IIBC) consistently interacted very specifically with SctG (Figure 3), despite low overall expression levels (Table S2). A closer look at the results also showed a significant enrichment of several components of the Lol protein export pathway for the insertion of lipoproteins into the OM, namely LolD and LolE, as well as other non-T3SS proteins, such as Lon protease (termed endopeptidase La in *Y. enterocolitica*) and the prokaryotic tubulin homolog FtsZ, a major player in cell division (Figure 3, Table S7).

Interestingly, PTS sugar transporters were shown to have a role in the regulation of the T3SS earlier (Mazé et al., 2014). We therefore constructed a clean *Δpts-IIBC* deletion mutant and tested its impact on assembly and function of the T3SS. A proteome analysis revealed that both the pilotin SctG and OmpW were among the few proteins significantly downregulated in *Δpts-IIBC* (Table S8), confirming the connection between the proteins. However, PTS-IIBC was not required for assembly of injectisomes or effector secretion (Figure S8a) and overexpression did not significantly impact T3SS localization or secretion itself (Figure S8b), leaving open the functional relevance of its interaction with the pilotin at this stage.
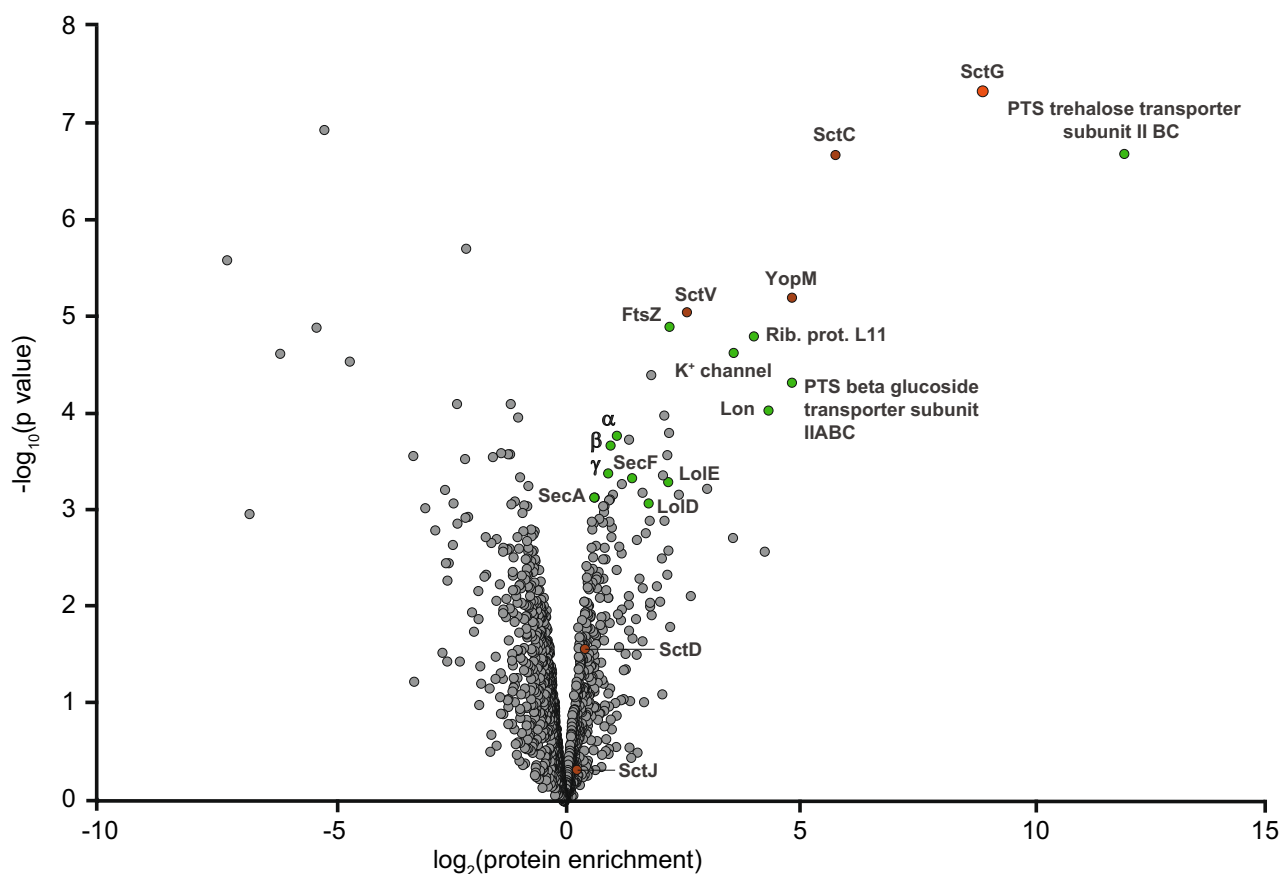
FIGURE 3 SctG interacts with T3SS components and additional non-T3SS proteins. Co-immunoprecipitation experiments with SctG-sfGFP as bait, compared to an unlabeled control strain expressing sfGFP from plasmid at comparable levels, both under non-secreting conditions. Interactors were quantified with label-free mass spectrometry (*n* = 3). The bait protein SctG is marked in orange, other T3SS components in dark red, interactors discussed in the main text in green. Greek letters denote subunits of the F1 subcomplex of the ATP synthase. A full list of all interactors with *p* < 0.001 can be found in Table S7.

2.4 | Pilotin expression is controlled by temperature, similar to structural T3SS components

To explain the significant interaction of SctG with non-T3SS components, we analyzed its expression and localization in more detail. Pilotin proteins are abundant but not omnipresent in secretin-containing secretion systems (Koo et al., 2012). Despite their consistently reported role for assembly of the highly conserved secretin, pilotins show low sequence conservation (Figure S9a). Accordingly, we found that even the pilotin from the closely related T3SS of *P. aeruginosa* could not complement a *sctG* deletion in *Y. enterocolitica* (Figure S9b).

Regardless of this low sequence conservation, pilotins have a conserved unique genetic location within the T3SS. In contrast to almost all other T3SS components, which are encoded in operons whose transcription is controlled by a common transcriptional regulator, pilotins are located in a joint operon upstream of this regulator (genetic neighborhood analysis, Figure S10). This arrangement might lead to faster expression of the pilotin in comparison to other T3SS components, which are activated by VirF itself. In addition, the presence of an RNA thermometer between *sctG* and *virF* (Böhme et al., 2012; Hoe & Goguen, 1993; Schwiesow et al., 2016) might lead to a specific pilotin expression profile.

SctG-sfGFP was expressed at a level below the detection limit prior to the shift to 37°C, which activates the VirF-dependent expression of other T3SS components. After the temperature shift, SctG expression increased steadily over the next two hours (Figure 4a,b). Overall, the SctG-sfGFP expression profile did not differ significantly from mCherry-SctD, a basal body protein labeled in the same strain (Figure 4b).

2.5 | T3SS-independent species-specific bacterial factors are required for the correct cellular localization of the pilotin

The functional SctG-sfGFP fusion allowed us to assay the cellular localization of SctG. To first test the requirement of other T3SS component or non-T3SS-related *Y. enterocolitica* proteins for SctG localization, SctG or SctG-sfGFP were expressed from plasmid in a *Y. enterocolitica* strain cured of the virulence plasmid (pYV−), as well as *Escherichia coli* Top10 (which has no T3SS) (Figure S11a). While SctG-sfGFP displayed a membrane localization in *Y. enterocolitica* pYV−, similar to its native localization, it localized predominantly to the cytosol in *E. coli* (Figure S11a,b). Notably, expression of SctG or SctG-sfGFP negatively influenced the growth of *E. coli*, which only
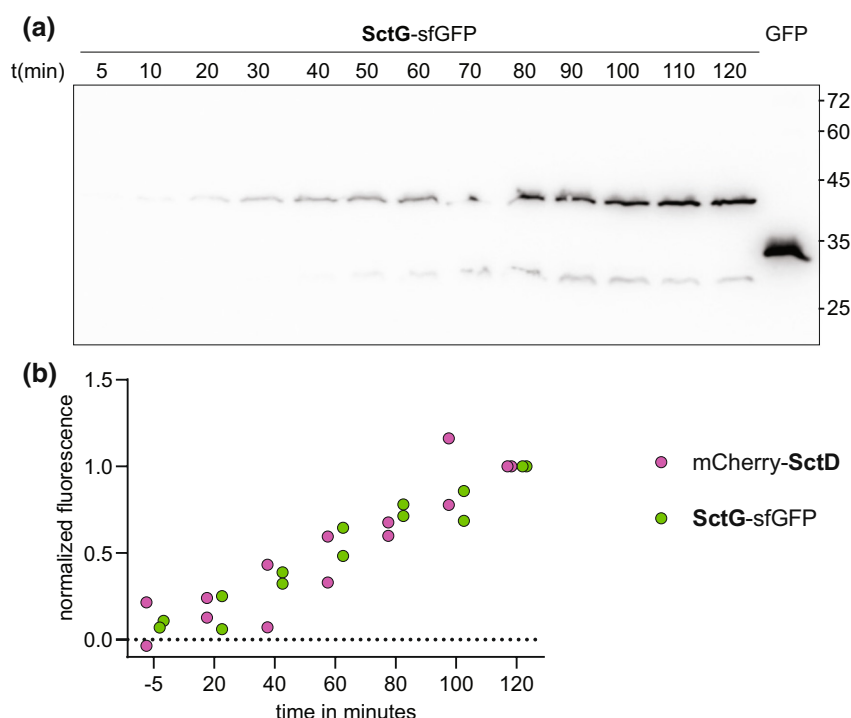
FIGURE 4 Despite its unique genetic location, SctG expression levels increase upon induction of T3SS expression, in a similar way as for other T3SS components. (a) Expression of SctG-sfGFP (expected molecular weight 42.2 kDa) expressed from the native genetic location in *Y. enterocolitica* under non-secreting conditions in rich medium. Immunoblot using antibodies directed against GFP. The band at an apparent molecular weight of 30 kDa, which develops similarly over time, may correspond to a degradation product of SctG-sfGFP or the product of an internal ribosome entry site at the N-terminus of sfGFP. Control: Expression of GFP from plasmid. Numbers indicate time in min relative to temperature shift to 37°C, which triggers the expression of T3SS components. Right, molecular weight in kDa. *n* = 2. (b) Expression of SctG-sfGFP and the IM ring component mCherry-SctD, both expressed from the native genetic location in *Y. enterocolitica*, before and after temperature shift to 37°C in a double-labeled strain under non-secreting conditions. Quantification of fluorescence per bacterium, normalized by the respective 120 min value. Dots indicate individual biological replicates with a total of 52, 100, 128, 128, 217, 185, 143 bacteria (from left to right).

reached a low OD. Microscopy experiments revealed severe lesions and plasmolysis in the respective bacteria (Figure S11a,c), indicating that the *Y. enterocolitica* pilotin mislocalizes and can thus be toxic upon ectopic expression in *E. coli*. Together, these data show that T3SS-independent species-specific bacterial factors are required for the membrane integration of the pilotin.

2.6 | Pilotins localize dynamically within the membrane and do not stably colocalize with other injectisome components

We then tested the localization of SctG-sfGFP expressed from its native genetic location in wild-type *Y. enterocolitica* with functional T3SS. To our surprise, we detected a disperse membrane localization of SctG-sfGFP, which increased over time, in addition to cytosolic background fluorescence (Figure 5a). While a certain clustering of SctG-sfGFP in the membrane was visible, these clusters did not visibly colocalize with the mCherry-labeled T3SS components SctC, SctD, or SctL, in contrast to the clear colocalization observed for mCherry-SctD and EGFP-SctQ used as positive control (Diepold et al., 2017) (Figures 5b and S12).

To analyze the mobility and cluster formation of SctG in more detail, we tracked SctG-sfGFP in individual bacteria. Still images and overlays (Figure 6a), as well as movies (Movie S1) showed that the localization of SctG and its clusters in the membrane strongly fluctuate, indicating diffusion within the membrane. We tested this hypothesis by fluorescence recovery after photobleaching (FRAP) experiments and found that indeed, SctG-sfGFP is highly mobile within the membrane with an average half-time of recovery at the bleached pole of 21.5 s (+/−13.0 s) (Figure 6b).

3 | DISCUSSION

Pilotin proteins are conserved components of T3SS in many bacteria including most animal pathogenic variants. They have a unique genetic location and a central role for the assembly of the T3SS injectisome. In this study, we confirm the role of pilotins in ensuring the proper localization and oligomerization of the secretin ring of the injectisome in the OM, but describe an additional specific effect on T3SS export substrate selection. Unexpectedly, we found that pilotins are mobile membrane components, raising the possibility that they have other cellular functions in addition to or after contributing to the assembly of the T3SS.

3.1 | Pilotins differentially affect major steps in T3SS assembly

Pilotins have long been known to assist the assembly of the SctC secretin ring in the OM (Burghout et al., 2004; Crago & Koronakis, 1998; Daefler & Russel, 1998; Koster et al., 1997; Perdu et al., 2015; Rau & Darwin, 2015; Schuch & Maurelli, 2001). Our data confirm these reports: In the absence of the pilotin, secretins localized in large foci at one of the bacterial poles in the majority (89.6%) of bacteria (Figure 2a). The localization of other T3SS components in absence of SctG differed from that of the secretin: SctL, a component of the cytosolic sorting platform of the T3SS, only occasionally (in 6.6% of the cells) formed single, mostly polar, foci. Similarly, we observed few, also mostly polar, needles for a subset of bacteria (4.6% of the cells). However, these needles and the sorting platform protein SctL did not colocalize (Figure S5b) like they do in wild-type cells (Diepold et al., 2010), indicating an absence of stably assembled injectisomes. Consistent with this, the nonameric large export apparatus component SctV (Abrusci et al., 2013) assembled, but moved within the membrane in the absence of SctG (Figures 2b and S5a), indicating a lack of anchoring by the ring-forming SctCDJ proteins (Diepold et al., 2011). We speculate that transient interactions of SctL and the other cytosolic T3SS components with basal body components at the poles might allow the limited export of the needle subunit. Once exported, these needles would stay stably associated with the bacteria despite the disassembly of the cytosolic sorting platform. In agreement with this hypothesis, we had found earlier that the cytosolic T3SS sorting platform components do exchange between the injectisome-bound sorting platform and a cytosolic pool (Diepold et al., 2015, 2017) and that the sorting platform components temporarily dissociate from the remaining injectisomes under certain conditions, such as low external pH (Wimmi et al., 2021). The presence of a low number of needles had previously been reported for the closely related *P. aeruginosa* T3SS (Perdu et al., 2015). Notably, the fraction of bacteria with associated needles and the overall secretion efficiency of the pilotin deletion showed an unusually high variation between individual replication experiments, in line with transient interaction or an influence of external factors. However, despite our best efforts, we were unable to identify these factors.

## 3.2 | Role of pilotins in T3SS substrate specificity

Analysis of the T3SS secretome by SDS-PAGE and quantitative mass spectrometry revealed a specific effect of the presence of the pilotin

FIGURE 5 SctG predominantly localizes in the membrane, but is not significantly enriched at injectisome sites. (a) Time course microscopy of SctG-sfGFP in *Y. enterocolitica* under non-secreting conditions. Time with reference to the temperature shift to 37°C. Bottom, intracellular localization of SctG-sfGFP at the respective time points. Line scans across single bacteria, approximate average positions of bacterial membranes (m., dark gray) and cytosol (beige) indicated. *n* = 78, 90, 81, 90 cells (left to right) from three independent biological replicates. (b) Colocalization of labeled T3SS components (all expressed from native genetic locus on virulence plasmid) in double-labeled strains as indicated, 120 min after temperature shift to 37°C. *n* = 3, except for colocalization of mCherry-SctD and EGFP-SctQ, which was reported earlier (Diepold et al., 2017) and included here as a positive control (*n* = 1). Scale bars = 2 μm.
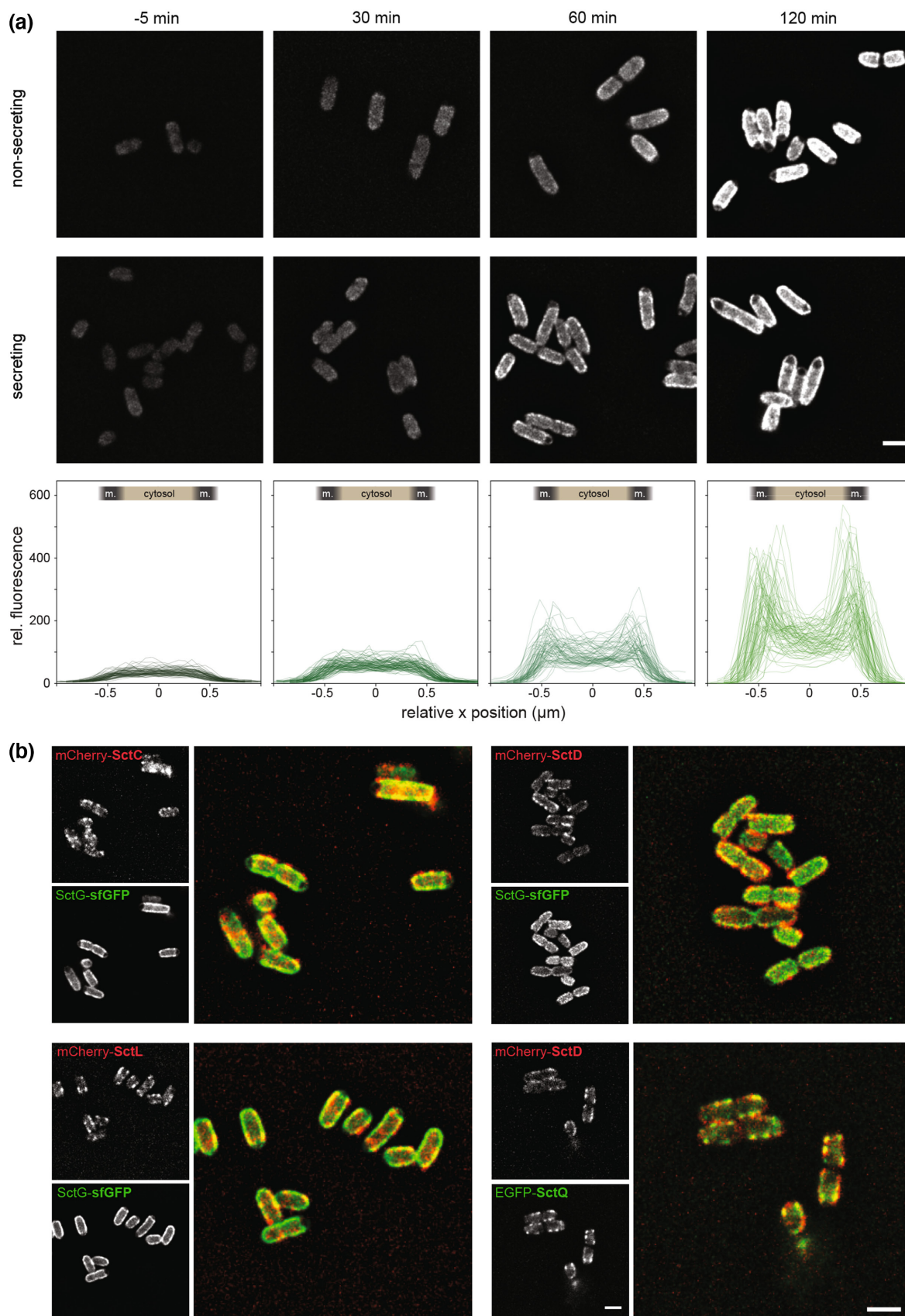
on export of the so-called early substrates, required for formation of the needle and its tip structure (Figure 1, Table 1). Although deletion or modifications of *sctG* have an effect on the expression of VirF and its targets (Tables S2 and S3), most likely due to an influence on the formation of hairpin structures in the *sctG-virF* mRNA that regulate VirF transcription as part of the thermoregulation of T3SS expression
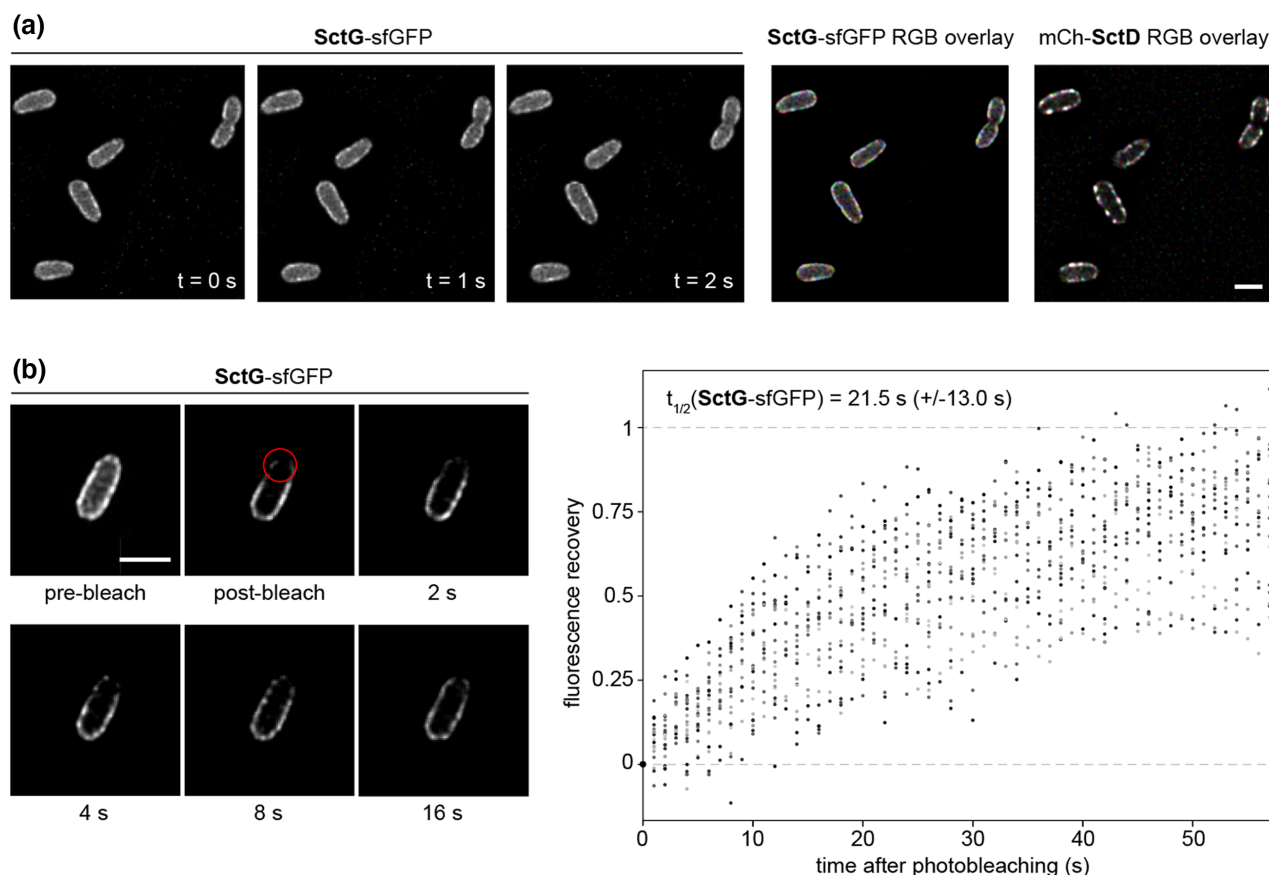
FIGURE 6 Pilotin proteins move dynamically within the membrane, forming transient patches. Fluorescence microscopy of a strain expressing SctG-sfGFP and mCherry-SctD from their native genetic locations on the virulence plasmid, incubated under non-secreting conditions. (a) Left, single micrographs of SctG-sfGFP taken with 1 s difference. Right, red/green/blue (RGB) overlay of those micrographs for SctG-sfGFP and mCherry-SctD (mCh-SctD) ($n=3$). (b) Fluorescence recovery after photobleaching for SctG-sfGFP. Left, representative individual micrographs before and at the indicated time points after the bleaching event. Bleach spot indicated by red circle. Right, quantification of fluorescence recovery after photobleaching ($n=21$ cells from 3 independent experiments, displayed in different shades of gray). The recovery half-time $t_{1/2}$ was calculated for each individual recovery curve (see Material and Methods for details) and is displayed as average with standard deviation.

(Böhme et al., 2012; Hoe & Goguen, 1993; Schwiesow et al., 2016), the role of SctG in secretion substrate is independent from VirF levels (Figures 1d and S4a; Table S4). This leaves open the reason for the striking change of substrate specificity in absence of the pilotin, where consistently and specifically, early export substrates are much more strongly affected by the absence of SctG than the late substrates, the virulence effectors. Notably, substrate-specific effects on the secretion had been found, although not always explicitly noted, in earlier studies in *Y. enterocolitica* (Allaoui et al., 1995; Burghout et al., 2004) and *P. aeruginosa* (Perdu et al., 2015). Taking into account the additional interactions of the pilotin that we observed, it is tempting to speculate that presence of the pilotin at the injectisome favors the secretion of early substrates. Subsequent dissociation of the pilotin would then contribute to a switch in export cargo specificity towards the effectors. The specific (albeit not necessarily direct) interaction of SctG with the large export apparatus component SctV (Figure 3), which is a key player in substrate selection (Bange et al., 2010; Inoue et al., 2021; Kinoshita et al., 2013; Minamino et al., 2020; Xing et al., 2018), supports this hypothesis.

In contrast, overexpression of SctG did not increase visibly the fraction of early substrates amongst the exported proteins (Figure S9b).

Alternative explanations for the change in export substrate specificity are (i) the polar localization of the secretin (and consequently any transient T3SS complex) in the absence of the pilotin, which might change the accessibility for certain substrates, or (ii) a two-step export pathway, with a first transport step across the IM, facilitated by the T3SS export apparatus (which is assembled, but not anchored in the peptidoglycan, in the absence of the pilotin (Figure 2b)) and a subsequent export step across the OM, facilitated by the secretin (without which no export is observed (Figure S2)). Such a two-step transport might prevent the export of early substrates, many of which polymerize outside the cytosol. Alternatively, (iii) the at most temporary association of the cytosolic components with the membrane components (Figure 2) could favor the export of late substrates, or (iv) strains lacking the pilotin might be able to provide less energy due to the missing link to the PTS sugar transporters (Figure 3) or membrane stress as a consequence of secretin misassembly. If effector export is less energy-costly than the export

of early substrates, this might explain the observed bias in export in absence of SctG. The observation that the intracellular levels of SctB (YopD) are slightly reduced in strains lacking SctG (Table S2), despite the lower secretion, argues against the hypothesis that SctB-induced turnover of *virF* mRNA, as shown in *Y. pseudotuberculosis* (Kusmierek et al., 2019), unspecifically reduces secretion in absence of the pilotin. Overall, in the absence of direct evidence for these alternative explanations, we consider a direct influence of SctG on the substrate specificity through interactions with other T3SS components to be the most likely explanation. It will be interesting to test these models in additional species like *S. flexneri*, where several studies indicate a stable stoichiometric interaction between pilotin and secretin after T3SS assembly (Flacht et al., 2023; Hu et al., 2015).

Substrate specificity switching is a central, but incompletely understood, feature type III secretion. Our data suggest that pilotin proteins play a key role in this process, together with the export apparatus components SctV and SctU (Sorg et al., 2007), the gatekeeper complex (Botteaux et al., 2009; Day & Plano, 1998) and the sorting platform (Lara-Tejero et al., 2011). If and how the interaction of the pilotin with the effector YopM (Figure 3) contributes to this process is unclear at the moment.

3.3 | Additional interactions of the pilotin and possible functions

An unexpected finding of our study was that pilotin concentrations significantly below wild-type levels are sufficient to restore normal T3SS assembly and function (Figure S6). SctG is one of the few T3SS machinery components encoded outside the VirF-regulated operons, and several factors were found to specifically influence VirF expression, including an RNA thermometer structure in the intergenic region between *sctG* and *virF* (Böhme et al., 2012; Kusmierek et al., 2019; Schwiesow et al., 2016). Nevertheless, native SctG expression levels increase over time after induction of the *yop* regulon by temperature shift to 37°C, similar to other T3SS components (Figure 4). This is consistent with the co-transcription of *sctG* and *virF* in one operon (Böhme et al., 2012) and a negligible lag phase between expression of VirF and its target proteins under the used conditions (incubation at 37°C prior to activation of secretion, which is expected to fully open the *sctG-virF* RNA thermometer structure (Böhme et al., 2012)). However, we found that low pilotin levels already were sufficient for injectisome assembly and secretion and that SctG-sfGFP expressed from the native promoter does not significantly colocalize with other T3SS components (Figure 5), but is highly mobile in the bacterial membrane (Figure 6). This suggests that besides its well-documented role as secretin receptor and assembly assistant, for which a low level of protein (which might already be present prior to the VirF-dependent upregulation of the remaining T3SS components) is sufficient, pilotins might have additional functions. We therefore screened for additional interactors of SctG by co-immunoprecipitation.

The most striking finding of the interaction studies was the highly specific enrichment of several PTS sugar transporter subunits, most significantly the membrane-bound trehalose transporter subunit EIIBC (Figure 3, Table S7). PTS systems are used for sugar uptake in many bacteria. They create a concentration gradient by transferring the PEP phosphoryl group onto the incoming sugar via several intermediate phosphate carriers. The EIIC subunit, which can be found expressed as a fusion to the EIIB subunit, serves as channel in the IM. While many bacteria express several PTS transporters, PTS are often unspecific and redundant (Jeckelmann & Erni, 2020). Notably, PTS were repeatedly found to act as carbohydrate sensors that control bacterial metabolism in response to the environment (Pflüger-Grau & Görke, 2010). Transporters sensing host-specific compounds can regulate expression and activity of virulence systems (Pacheco & Sperandio, 2015), indicating that SctG and its most highly enriched interactor, the PTS trehalose transporter subunit EIIBC, might serve to modulate T3SS function according to the bacterial environment. Indeed, PTS systems were repeatedly associated with bacterial virulence (reviewed in Jeckelmann & Erni, 2019, 2020): amongst others, presence of the PTS glucose transporter subunit EIIBC conferred a competitive advantage to *Y. pestis* in serum-like medium (Palace et al., 2014), a *Vibrio cholerae* PTS system was found to modulate virulence gene expression (Wang et al., 2015), and *Salmonella* Typhimurium lacking a PTS EI subunit showed a nearly 1000-fold increase in LD_{50} (Kok et al., 2003). Specifically a PTS trehalose transporter system induces hypervirulence in *Clostridium difficile* (Collins et al., 2018). Notably, the PTS glucose transporter EIIA subunit directly interacts with cytosolic components of the *Salmonella* SPI-2 T3SS and activates type III secretion (Mazé et al., 2014). Our experiments failed to show a direct link between the PTS trehalose transporter subunit EIIBC and T3SS assembly and activity. Overall, the two most likely links between PTS sugar transporters and virulence appear to be energy provision and/or host sensing. The fact that so far, no pilotin homologs were found in plant pathogens (Büttner, 2012), is consistent with this hypothesis; further experiments are required to describe the connection in more detail. Notably, absence of both the secretin SctG and the interacting PTS trehalose transporter subunit EIIBC led to a reduced cellular amount of OmpW, an eight-stranded beta-barrel OM protein required for resistance to phagocytosis in *E. coli* (Albrecht et al., 2006; Hong et al., 2006; Wu et al., 2013) (Tables S2 and S6). While the coordination of the anti-phagocytic actions of OmpW and *Y. enterocolitica* T3SS effectors appears intuitively beneficial for the bacteria during infections, OmpW itself was not found to interact with SctG and the functional interaction remains unclear for the moment.

Notably, while the pilotin mostly fractionates with the OM in membrane preparations (Burghout et al., 2004; Rau & Darwin, 2015; Schuch & Maurelli, 1999), many of the proteins found to interact with the labeled pilotin in the co-immunoprecipitation assay are integral IM proteins or IM-associated proteins. The used SctG-sfGFP fusion is expressed from its native genetic location, supports native secretion (Figure S7a,b), and interacts with both known interactors, the secretin SctC and proteins of the Lol pathway, in our assays (Figure 3). While these are strong indications for correct localization and interactions of SctG-sfGFP, it is possible that transport of the fusion protein to the OM is impaired (or the observed slightly increased levels of SctG-sfGFP saturate the export pathways to the OM), which in

turn may enhance the fraction of pilotins that can contact these IM(-associated) proteins. Alternatively, the interactions may be caused by natively soluble pilotin proteins, possibly bound to other proteins such as LolB (Majewski et al., 2021; Okon et al., 2008). Finally, the N-terminal lipid anchor of the pilotin might be removed after assembly of the secretin ring or the injectisome, which would render the protein soluble (Burghout et al., 2004) in the periplasm.

Other significant interaction partners of the pilotin outside the T3SS are FtsZ, a prokaryotic tubulin homolog with a key role in cell division, the protease Lon, components of the ATP synthase (subunits α, β, γ), the Sec export pathway (SecF/A), and LolD/E, two components of the ABC transporter of the Lol lipoprotein export pathway in the IM. FtsZ is an interesting interactor, as it might play a role in the long-known, but still incompletely understood link between T3SS activity and cell growth and division (actively secreting bacteria of many species cease growth and division and are often bigger than T3SS-deficient or non-secreting bacteria (Carter et al., 1980; Milne-Davies et al., 2019; Sasakawa et al., 1986; Sturm et al., 2011)). Notably, although pilotin mutants secrete effectors, they display no secretion-associated growth inhibition (Figure S4b). This is in line with the hypothesis that binding of FtsZ by the pilotin at least contributes to the secretion-associated growth inhibition. However, since overall secretion levels are reduced in the *sctG* mutant, a role of the energetic cost of production and secretion of T3SS substrates cannot be excluded by these experiments. Since to our knowledge, this is the first time that a T3SS component was found to be associated with bacterial cytoskeleton proteins, this might also indicate an involvement of SctG in the non-random localization of T3SS around the cell found for *Y. enterocolitica* (Kudryashev et al., 2015). The Lon protease degrades unfolded or misfolded proteins, especially under stress conditions (Gur & Sauer, 2008), but can also have more specific roles in metabolism, cell cycle control, and virulence through proteolysis of specific regulatory proteins (Omnus et al., 2021; Tsilibaris et al., 2006). While it cannot be ruled out that the specific interaction of SctG-sfGFP with Lon denotes degradation of partially misfolded protein, Lon proteases have been shown to influence T3SS activity, both positively via degradation of histone-like proteins like *Yersinia* YmoA that suppress the transcription of T3SS components (Breidenstein et al., 2012; Cornelis, 1993; Cornelis et al., 1991; Jackson et al., 2004) and negatively, most likely by directly degrading key components of the T3SS, mainly in plant pathogens (Bretz et al., 2002; Figaj et al., 2020; Lee et al., 2018; Zhou et al., 2018). The presence of three components of the IM ATP synthase amongst the less than forty specific interactors of the pilotin protein is remarkable and, in combination with the strong interaction with the PTS sugar transporter, suggests a link with the bacterial energy metabolism. While such a link is more than conceivable, given the high energy expense of type III secretion (Renault et al., 2019), its details are unclear at the moment. As lipoproteins in the OM, pilotins are expected to interact with components of both the Sec and the Lol pathway (Collin et al., 2011; Konovalova & Silhavy, 2015; Okon et al., 2008). While most models emphasize the interaction with LolA and LolB in the periplasm and OM, respectively, we detected strong binding to LolD and LolE in the IM (Figure 3, Table S7). Of the two models proposed for the role of pilotins in the

assembly of the secretin ring by Majewski and colleagues (Majewski et al., 2021), our data therefore supports the second model where the pilotin is released from LolB before interacting with the secretin. Interestingly, in addition to plant pathogenic T3SS, some animal pathogenic T3SS do not have a known pilotin, notably the T3SS of enteropathogenic and enterohemorrhagic *Escherichia coli* (EPEC/EHEC) and *Salmonella* SPI-2. It is conceivable that these T3SS do not rely on potential roles of the pilotin discussed above, such as energy sensing or contribution to the specific localization of the injectisome. In any case, the role of the pilotin in ensuring the proper assembly and localization of the secretin ring in the OM is probably taken over by SctD or other accessory proteins in these bacteria, as is the case for other T2SS/T3SS secretins (Koo et al., 2012) and was specifically shown for the EPEC T3SS (Tseytin et al., 2017).

Taken together, our data indicate that, besides their function in the assembly of the secretin ring of the T3SS, pilotin proteins may have additional roles linked to type III secretion. In their absence, assembly of all T3SS subcomplexes and specifically the export of early secretion substrates is strongly impeded, while effectors are exported efficiently. Pilotin proteins interact with components of the T3SS, most prominently the secretin SctC and the large export apparatus component SctV. However, these interactions may be in a dynamic equilibrium (Collin et al., 2013), as the majority of pilotin proteins are mobile in the bacterial membrane and do not stay attached to or even significantly colocalize with the injectisome. In line with these findings, SctG also specifically interacted with other cell wall-associated proteins such as a PTS sugar transporter subunit.

A potential model integrating these findings is that during injectisome assembly, the pilotin interacts with the secretin SctC and facilitates its oligomerization in the OM. The presence of the pilotin supports the export of early secretion substrates, which are required for needle formation. At a later time point, SctG may at least partially dissociate from the fully assembled injectisome, in line with its absence in fully assembled SPI-1 injectisomes (Hu et al., 2017), which then would favor the export of effector proteins upon activation of the T3SS. The pilotin is mobile at this stage and may additionally contribute to efficient secretion by interacting with other partners, including PTS sugar transporters, which could provide the necessary energy for secretion. Such species-specific functions would be in line with the observed differences between species in localization of the pilotin protein after T3SS assembly (Flacht et al., 2023; Hu et al., 2015, 2017, 2018; Miletic et al., 2021). Challenging this model in future studies will lead to a better understanding of the role of pilotins in both assembly and function of the T3SS.

4 | MATERIALS AND METHODS

4.1 | Bacterial strain generation and genetic constructs

A list of strains and plasmids used in this study can be found in Table S9. All *Y. enterocolitica* strains used in this study are based on the *Y. enterocolitica* wild-type strain MRS40 or its derivate IML421asd

(ΔHOPEMTasd). In IML421asd all major virulence effector proteins (YopH,O,P,E,M,T) are absent. Furthermore, this strain harbors a deletion of the aspartate-beta-semialdehyde dehydrogenase gene, which renders the strain auxotrophic for diaminopimelic acid (DAP), making it suitable for work in a biosafety class 1 environment (Kudryashev et al., 2013). Modifications and deletions of genes on the *Yersinia* virulence plasmid were introduced by allelic exchange (Kaniga et al., 1991).

4.2 | Bacterial cultivation, secretion assays, and protein analysis

Y. enterocolitica day cultures were inoculated from fresh stationary overnight cultures supplemented with nalidixic acid (35 mg/mL) and DAP (60 μg/mL), where required, to an OD_{600} of 0.15 for secreting and 0.12 for non-secreting conditions, respectively. To select for the maintenance of expression plasmids, ampicillin was added (0.2 mg/mL). As rich medium, BHI (brain heart infusion broth), supplemented with nalidixic acid (35 mg/mL), DAP (60 μg/mL), where required, glycerol (0.4%) and $MgCl_2$ (20 mM) was used. As minimal medium, microscopy medium (100 mM 2-[4-(2-Hydroxyethyl)piperazin-1-yl]ethane-1-sulfonic acid (HEPES) pH 7.2, 5 mM $(NH_4)_2SO_4$, 100 mM NaCl, 20 mM sodium glutamate, 10 mM $MgCl_2$, 5 mM K_2SO_4, 50 mM 2-(N-morpholino)ethanesulfonic acid (MES), 50 mM glycine), supplemented with nalidixic acid (35 mg/mL), 0.5% casamino acids, DAP (60 μg/mL), where required, glycerol (0.4%) and $MgCl_2$ (20 mM) was used. For secreting conditions, 5 mM EGTA was added; for non-secreting conditions, 5 mM $CaCl_2$ was added to the pre-warmed (approx. 55°C) medium, which was filtered through a 0.45 μm filter before the addition of other supplements and cooled down to ambient temperature for the experiments. After inoculation, day cultures were incubated at 28°C for 90 min to reach exponential growth phase. Expression of the *yop* regulon was then induced by a rapid temperature shift to 37°C in a water bath. Where indicated, protein expression from plasmid (derivates of pBAD-His/B (Invitrogen)) was induced at this point by the addition of L-arabinose (0.2%, unless indicated differently). As an exception, expression of VirF from pCL5 (Lambert de Rouvroit et al., 1992) was induced by addition of isopropyl β-D-1-thiogalactopyranoside (IPTG), as indicated in the figure legend.

For protein secretion assays and analysis of total cellular proteins, bacteria were incubated for 150–180 min at 37°C, unless indicated otherwise. 2 mL of the culture was collected at 21,000 g for 10 min. Where bovine serum albumin (BSA) was used as a loading control, 2 μg was added before centrifugation. The supernatant was removed from the total cell pellet and proteins were precipitated by addition of a final concentration of 10% trichloroacetic acid (TCA) and incubation at 4°C for 1–8 h. Precipitated proteins were collected by centrifugation for 15 min at 21,000 g and 4°C, the pellet was washed once with 1 mL ice-cold acetone and subsequently resuspended in SDS-PAGE loading buffer. Total cellular protein samples were normalized to 0.3 OD units (ODu, 1 Odu is equivalent to 1 mL of culture at on OD_{600} of 1, corresponding to approximately 5×10^8 *Y. enterocolitica*) and supernatant samples to the equivalent of 0.6 Odu. Before loading, samples were incubated for 5 min at 99°C. Separation was performed on 11%, 15%, or gradient 12%–20% SDS-PAGE gels, using BlueClassic Prestained Marker (Jena Biosciences) as a size standard. For visualization, the SDS-PAGE gels were stained with InstantBlue (Expedeon). For immunoblots, the separated proteins were transferred from the SDS-PAGE gel onto a nitrocellulose membrane. Primary mouse antibodies against GFP (Thermo Fisher Proteintech 66,002-1-Ig, 1:4000) were used in combination with secondary anti-mouse antibodies conjugated to horseradish peroxidase (GE Healthcare NXA931, 1:5000); primary polyclonal rabbit antibodies against SctA (LcrV) (MIPA220, 1:2000), SctF (MIPA223, 1:1000) and YscX (MIPA224, 1:500) were used in combination with secondary anti-rabbit antibodies conjugated to horseradish peroxidase (Sigma A8275, 1:5000). For visualization, ECL chemiluminescence substrate (Pierce) was used in a LAS-4000 Luminescence Image Analyzer.

4.3 | Fluorescence microscopy

For fluorescence microscopy, bacteria were treated as described above. After 150–180 min at 37°C, 400 μL of bacterial culture was collected by centrifugation (2400 g, 2 min) and reconstituted in 200 μL microscopy medium. 2 μL of resuspension was spotted on agarose pads (1.5% low melting agarose (Sigma-Aldrich) in microscopy medium) in glass depression slides (Marienfeld). Where required, agarose pads and media were supplemented with 60 μg/mL DAP for ΔHOPEMTasd-based strains, 5 mM $CaCl_2$ for non-secreting conditions, or 5 mM EGTA for secreting conditions.

Microscopy was performed on a Deltavision Elite Optical Sectioning Microscope equipped with an UPlanSApo 100×/1.40 oil objective (Olympus), using an Evolve EMCCD camera (Photometrics). Where applicable, the prepared samples were illuminated first in the mCherry = 0.4 s with a mCherry filter set and afterward in GFP = 0.2 s with a GFP filter set. Depending on the experiment, z stacks with 1–15 slices (Δz = 0.15 μm) per fluorescence channel were acquired. The acquired micrographs were subsequently deconvolved using softWoRx 7.0.0 (standard "conservative" settings). Images were further processed with FIJI (ImageJ 1.51f/1.52i/1.52n) (Schindelin et al., 2012). Where necessary, a drift correction with the StackReg Plugin (Thevenaz et al., 1998) was performed. Fluorescence quantification was performed in FIJI. For presentation of micrographs in a figure, representative fields of view were selected, and brightness and contrast of the micrographs was adjusted identically within the compared image sets.

4.4 | Maleimide-based needle (SctF) staining

Maleimide-based staining to visualize the injectisome needles was performed as described in (Wimmi et al., 2021). Briefly, expression of SctF$_{S5C}$ from the pBAD-His/B plasmid was induced by addition of 1.0% L-arabinose at the time of the temperature shift in strains expressing the native SctF at the same time. After 150–180 min, bacteria were collected and resuspended in 0.2 volumes of

microscopy medium supplemented with $5\,\mu M$ CF 488A maleimide dye (Sigma-Aldrich, USA) at 37°C for 5 min. After staining, cells were washed once with $1500\,\mu L$ of microscopy medium and resuspended in $200\,\mu L$ of microscopy medium. $2\,\mu L$ of bacterial suspension was spotted on 1.5% agarose pads in microscopy medium and visualized under the microscope as described above.

4.5 | Classification and quantification of fluorescent foci

To determine the number of stable SctV-EGFP foci, seven micrographs were taken in 15 s intervals and the minimal intensity for each location was determined from the deconvoluted micrographs. Foci were then identified in FIJI using an intensity threshold of 700 (determined in images of the wild-type background strain) and the "analyze particles" function with a minimal size of 4 pixels and a particle circularity of 0.5–1.0. To evaluate the fraction of bacteria with foci for SctC-mCherry, mCherry-SctL, and SctF$_{S5C}$ in the absence of SctG, foci were manually identified and classified as polar, subpolar, and lateral based on their subcellular localization in deconvoluted micrographs. In case a cell displayed multiple foci in different localization classes, bacteria were classified as containing a lateral, subpolar, polar focus in descending order (e.g. a bacterium with a lateral and a polar focus was assigned "lateral"). To determine the fraction of bacterial with stable foci for SctV-mCherry, foci were identified as described above, but not classified based on their location. The overall number of bacteria in a field of view was determined by using the deep learning-based network, DeepBacs (Spahn et al., 2021), that was previously trained with differential interferometry contrast (DIC) micrographs of *Y. enterocolitica*. The overall percentage of cells with foci is displayed in the figure.

4.6 | Fluorescence distribution analysis

For analysis of the fluorescence distribution across bacteria, line scan analysis was performed on deconvoluted micrographs in FIJI. With the straight line freehand tool, measurement areas were defined from one lateral membrane to the other at a 90° angle. Per condition, 3 fields of view with 18–30 cells were analyzed and the background was measured. The line scans were individually corrected for background fluorescence, normalized (fluorescence fraction relative to overall fluorescence over background) and centered at the position closest to the center of the total fluorescence over background.

4.7 | Fluorescence recovery after photobleaching (FRAP)

Cells were grown in non-secreting medium as described above. Samples were taken after 3 h at 37°C. To minimize unnecessary

bleaching, no z stacks were acquired. Three pre-bleach images were acquired and locations near selected bacterial cell poles were photobleached by individual 30 ns pulses of a 488 nm laser. Recovery of the bleached foci was followed by time-lapse microscopy. Deconvolved micrographs were used for the fluorescence quantification.

The relative fluorescence of the bleached spot was calculated as follows:

$$\text{Relative fluorescence} = \frac{(\text{Intensity bleached cell pole} - \text{Intensity background})}{(\text{Intensity total cell} - \text{Intensity background})}.$$

The relative fluorescence was then normalized (average prebleach value set to 1; post-bleach value set to 0), and an exponential recovery was fitted using the equation:

$$y = A\left(1 - e^{-bx}\right),$$

where y stands for the relative fluorescence, x for the time, A for the overall ratio of fluorescence recovery, and b for the inverse of the time constant $\tau_{1/2}$. For the fit, A was restricted to values between 0.7 and 1.1. Each bleach curve was fitted individually, and fits with $R^2 < 0.7$ were excluded from further analysis. The half-time of recovery was calculated from the time constant as follows:

$$t_{1/2} = \ln(2)\tau_{1/2.}$$

4.8 | Proteome and secretome analysis by shotgun proteomics-based mass spectrometry

Strains were grown and prepared as described above, under secreting conditions, unless mentioned otherwise. After 150 min at 37°C, cultures were normalized to an OD_{600} of 0.5, and 2 mL were harvested by centrifugation at $9391\,g$ for 2 min. Cell were washed 3 times with phosphate-buffered saline (PBS) (8 g/L NaCl, 0.2 g/L KCl, 1.78 g/L $Na_2HPO_4*2H_2O$, 0.24 g/L KH_2PO_4, pH 7.4). After washing, the cell pellet was resuspended in $300\,\mu L$ lysis buffer (2% sodium lauroyl sarcosinate (SLS), 100 mM ammonium bicarbonate (ABC)) and incubated at 90°C for 10 min. Protein concentrations were measured using a BCA assay (Thermo Scientific) and following reduction in 5 mM Tris(2-carboxyethyl)phosphin (TCEP, 15 min at 90°C) and alkylation in 10 mM iodoacetamide (30 min, 20°C in the dark), $50\,\mu g$ protein was used for tryptic digestion (1 μg, Serva) at 30°C overnight in presence of 0.5% SLS. After digestion, SLS was precipitated by adding a final concentration of 1.5% trifluoroacetic acid (TFA).

Desalting of cleared peptide samples was performed in C18 solid phase extraction (SPE) cartridges (Macherey-Nagel). First, cartridges were prepared by adding acetonitrile, followed by equilibration using 0.1% TFA and loading of peptide samples. Cartridges were washed with buffer containing 5% acetonitrile and 0.1% TFA, and finally eluted with 50% acetonitrile and 0.1% TFA into a fresh tube. Eluted peptides were dried and reconstituted in 0.1% TFA for LC–MS analysis.

Purified peptides were analyzed by liquid chromatography-mass spectrometry (MS) carried out on a Q-Exactive Plus instrument

connected to an Ultimate 3000 rapid-separation liquid chromatography (RSLC) nano instrument and a NanoSpray Flex Ion Source (all Thermo Scientific). Peptide separation was performed on a reverse-phase high-performance liquid chromatography (HPLC) column (75 μm by 42 cm) packed in-house with C_{18} resin (2.4 μm; Dr. Maisch GmbH). The peptides were first loaded onto a C18 precolumn (preconcentration set-up) and then eluted in backflush mode with a gradient from 98% solvent A (0.15% formic acid) and 2% solvent B (99.85% acetonitrile, 0.15% formic acid) to 25% solvent B over 66 min, continued from 25% to 40% of solvent B up to 90 min. The flow rate was set to 300 nL/min. The data acquisition mode for label-free quantification (LFQ) was set to obtain one high-resolution MS scan at a resolution of 70,000 (m/z 200) with scanning range from 375 to 1500 m/z followed by MS/MS scans of the 10 most intense ions at a resolution of 17,500. To increase the efficiency of MS/MS shots, the charged state screening modus was adjusted to exclude unassigned and singly charged ions. The dynamic exclusion duration was set to 10 s. The ion accumulation time was set to 50 ms (both MS and MS/MS). The automatic gain control (AGC) was set to 3×10^6 for MS survey scans and 1×10^5 for MS/MS scans.

Due to an instrument upgrade, the Q Exactive Plus system was replaced by an Exploris 480 mass spectrometer (Thermo Scientific). For total proteome analysis, purified peptides were analyzed using identical LC settings, and the Exploris MS data acquisition settings were the following: one high-resolution MS scan at a resolution of 60,000 (m/z 200) was obtained with scanning range from 350 to 1650 m/z followed by MS/MS scans of 2 s cycle time at a resolution of 15,000. Charge state inclusion was set between 2 and 6. The dynamic exclusion duration was set to 14 s. The ion accumulation time was set to 25 ms for MS and AUTO for MS/MS. The automatic gain control (AGC) was set to 300% for MS survey scans and 200% for MS/MS scans.

LFQ analysis was performed using MaxQuant (Cox & Mann, 2008) in standard settings using a *Y. enterocolitica* protein database containing proteins of the closely related *Y. enterocolitica* strain W22703 (Fuchs et al., 2011) and of the pYVe227 virulence plasmid (GenBank entry AF102990.1). Statistical follow-up analysis of the MaxQuant LFQ data was performed on an updated SafeQuant (Ahrné et al., 2016; Glatter et al., 2012) R-script modified to routinely process MaxQuant "protein groups" outputs. The missing value imputation was adapted from Perseus (Tyanova et al., 2016) in default settings and implemented into the updated SafeQuant script. Unless otherwise indicated, proteins with ≥3 detected peptides and a p value ≤0.01 of the sample versus the control using Student's t-test were considered as enriched and displayed in the tables. Intensity values were shaded according to their value (blue for high intensity; transparent for low intensity) for easier visualization.

For secretome analysis and quantification of secreted effectors in supplemented microscopy medium, 5 mL BHI cultures were grown under secreting conditions in 15 mL tubes as otherwise described before. After two hours of incubation at 37°C, the medium was changed from BHI to supplemented microscopy medium. Next, bacteria were again incubated at 37°C shaking for one hour. Samples were OD-normalized in a 2 mL volume, and bacteria were removed

by centrifugation (10 min at 21,000 g, 4°C). In the next step, the supernatant was removed and precipitated with a final concentration of 10% TCA for 1–8 h at 4°C; proteins were collected by centrifugation for 15 min at 21,000 g at 4°C and washed once with 1 mL ice-cold acetone. A detailed description of the experimental procedure is shown in (Lampaki et al., 2020). The remaining pellet was resuspended in 300 μL lysis buffer and incubated at 90°C for 10 min. Following reduction and alkylation (see above), proteins were digested using 1 μg trypsin. All further steps including C18-SPE, LC–MS analysis, and LFQ data analysis were identical to the ones described above. The LC separating gradient length was reduced to 45 min due to lower sample complexity.

4.9 | Co-immunoprecipitation and shotgun proteomics

For co-immunoprecipitation, 100 mL of non-secreting culture medium was inoculated to an OD_{600} of ~0.15 and treated as described above. After 2.5 h incubation at 37°C, the cultures were transferred to 50 mL tubes and centrifuged at 2000 g for 15 min at 4°C. Pellets were washed with 10 mL of 1x PBS. The contents of two tubes were pooled and centrifuged at 2000 g for 15 min at 4°C. The pellet was resuspended in 2 mL HNN lysis buffer (50 mM HEPES pH 7.5, 150 mM NaCl, 50 mM NaF, sterile filtered; protease inhibitor (cOmplete Mini, EDTA free (Roche)) added before use) and incubated for 30 min on a turning wheel at 4°C. Afterward, the bacteria were sonicated with 12 pulses à 30 s in a Hielscher UP200ST ultrasonic homogenizer. The cells were again placed on a turning wheel for 30 min at 4°C, and the sonication process and the subsequent incubation on a turning wheel were repeated. Unbroken cells were removed by centrifugation (20,000 g, 20 min, 4°C). For affinity purification, 10 μL of bead slurry (GFP-Trap Magnetic Agarose, ChromoTek) was added to the lysate and incubated shaking for 1 h at 4°C on a turning wheel. Beads were washed with 500 μL HNN lysis buffer + 0.1% NP40, followed by seven consecutive washing steps with 700 μL 100 mM ABC. 200 μL of elution buffer (100 mM ABC, 1 μg trypsin per sample) was added to the beads and incubated for 45 min on a thermomixer at 30°C at 1200 rpm. Beads were separated and the supernatant was collected. Beads were washed twice using 80 μL of elution buffer 2 (1 M urea, 100 mM ABC, 5 mM TCEP), combined with the first eluate fraction, and incubated o/n at 30°C to complete proteolysis. To monitor the experimental steps, samples for Western blot analysis were taken throughout the whole procedure. After digestion, 10 mM iodoacetamide was added and the samples were incubated for 30 min in the dark. For desalting, C18 solid phase extraction cartridge samples were acidified and the procedure was carried out as described above. The samples were analyzed on a Q Exactive Plus mass spectrometer using a resolving LC gradient of 40 min. The analytical settings and data analysis steps including MaxQuant and SafeQuant are described above. Unless otherwise indicated, proteins with ≥3 detected peptides and a p value ≤0.001 of the sample versus the control using Student's t-test were considered as enriched and displayed in the tables.

4.10 | Sequence analysis

For the analysis of the genetic environment of T3SS pilotin proteins from model organisms, the following GenBank sequences were used: AF102990.1 (*Yersinia enterocolitica* plasmid pYVe227, complete sequence), NC_002516.2 (*Pseudomonas aeruginosa* PAO1, complete genome reference sequence), NC_003197.2 (*Salmonella enterica* subsp. *Enterica* serovar Typhimurium str. LT2, complete genome reference sequence), NC_004851.1 (*Shigella flexneri* 2a str. 301 plasmid pCP301, complete sequence), AM286415.1 (*Yersinia enterocolitica* subsp. *Enterocolitica* 8081, complete genome). Multiple sequence alignment of the *sctG* and *sctC* genes of the same systems was performed using T-COFFEE 11.0 (Wallace et al., 2006).

CONFLICT OF INTEREST STATEMENT

The authors declare no competing interests.

DATA AVAILABILITY STATEMENT

The data that support the findings of this study are available from the corresponding author upon reasonable request.

ETHICS STATEMENT

None.

ORCID

Andreas Diepold https://orcid.org/0000-0002-4475-3923

REFERENCES

Abby, S.S. & Rocha, E.P.C. (2012) The non-flagellar type III secretion system evolved from the bacterial flagellum and diversified into host-cell adapted systems. *PLoS Genetics*, 8, e1002983.

Abrusci, P., Vergara-Irigaray, M., Johnson, S., Beeby, M.D., Hendrixson, D.R., Roversi, P. et al. (2013) Architecture of the major component of the type III secretion system export apparatus. *Nature Structural & Molecular Biology*, 20, 99–104.

Ahrné, E., Glatter, T., Viganò, C., Von Schubert, C., Nigg, E.A. & Schmidt, A. (2016) Evaluation and improvement of quantification accuracy in isobaric mass tag-based protein quantification experiments. *Journal of Proteome Research*, 15, 2537–2547.

Albrecht, R., Zeth, K., Söding, J., Lupas, A. & Linke, D. (2006) Expression, crystallization and preliminary X-ray crystallographic studies of the outer membrane protein OmpW from *Escherichia coli*. *Acta Crystallographica. Section F, Structural Biology and Crystallization Communications*, 62, 415–418.

Allaoui, A., Scheen, R., Lambert de Rouvroit, C. & Cornelis, G.R. (1995) VirG, a *Yersinia enterocolitica* lipoprotein involved in Ca2+ dependency, is related to exsB of *Pseudomonas aeruginosa*. *Journal of Bacteriology*, 177, 4230–4237.

Bange, G., Kümmerer, N., Engel, C., Bozkurt, G., Wild, K. & Sinning, I. (2010) FlhA provides the adaptor for coordinated delivery of late flagella building blocks to the type III secretion system. *Proceedings of the National Academy of Sciences of the United States of America*, 107, 11295–11300.

Blocker, A.J., Gounon, P., Larquet, E., Niebuhr, K., Cabiaux, V., Parsot, C. et al. (1999) The tripartite type III secreton of *Shigella flexneri* inserts IpaB and IpaC into host membranes. *The Journal of Cell Biology*, 147, 683–693.

Böhme, K., Steinmann, R., Kortmann, J., Seekircher, S., Heroven, A.K., Berger, E. et al. (2012) Concerted actions of a thermo-labile regulator and a unique intergenic RNA thermosensor control Yersinia virulence. *PLoS Pathogens*, 8, e1002518.

Botteaux, A., Sory, M.-P., Biskri, L., Parsot, C. & Allaoui, A. (2009) MxiC is secreted by and controls the substrate specificity of the *Shigella flexneri* type III secretion apparatus. *Molecular Microbiology*, 71, 449–460.

Breidenstein, E.B.M., Janot, L., Strehmel, J., Fernandez, L., Taylor, P.K., Kukavica-Ibrulj, I. et al. (2012) The Lon protease is essential for full virulence in *Pseudomonas aeruginosa*. *PLoS One*, 7, e49123.

Bretz, J., Losada, L., Lisboa, K. & Hutcheson, S.W. (2002) Lon protease functions as a negative regulator of type III protein secretion in *Pseudomonas syringae*. *Molecular Microbiology*, 45, 397–409.

Burgess, J.L., Case, H.B., Burgess, R.A. & Dickenson, N.E. (2020) Dominant negative effects by inactive Spa47 mutants inhibit T3SS function and Shigella virulence. *PLoS One*, 15, e0228227.

Burghout, P., Beckers, F., de Wit, E., van Boxtel, R., Cornelis, G.R., Tommassen, J. et al. (2004) Role of the pilot protein YscW in the biogenesis of the YscC secretin in *Yersinia enterocolitica*. *Journal of Bacteriology*, 186, 5366–5375.

Burkinshaw, B.J. & Strynadka, N.C. (2014) Assembly and structure of the T3SS. *Biochimica et Biophysica Acta (BBA)—Molecular Cell Research*, 1843, 1648–1693.

Büttner, D. (2012) Protein export according to schedule: architecture, assembly, and regulation of type III secretion systems from plant- and animal-pathogenic bacteria. *Microbiology and Molecular Biology Reviews*, 76, 262–310.

Carter, P.B., Zahorchak, R.J. & Brubaker, R.R. (1980) Plague virulence antigens from *Yersinia enterocolitica*. *Infection and Immunity*, 28, 638–640.

Chakravortty, D., Rohde, M., Jäger, L., Deiwick, J. & Hensel, M. (2005) Formation of a novel surface structure encoded by Salmonella Pathogenicity Island 2. *The EMBO Journal*, 24, 2043–2052.

Chami, M., Guilvout, I., Gregorini, M., Rémigy, H.W., Müller, S.A., Valerio, M. et al. (2005) Structural insights into the secretin PulD and its trypsin-resistant core. *The Journal of Biological Chemistry*, 280, 37732–37741.

Chernyatina, A.A. & Low, H.H. (2019) Core architecture of a bacterial type II secretion system. *Nature Communications*, 10, 1–10.

Coombes, B.K. (2009) Type III secretion systems in symbiotic adaptation of pathogenic and non-pathogenic bacteria. *Trends Microbiol*, 17, 89–94.

Collin, S., Guilvout, I., Nickerson, N.N. & Pugsley, A.P. (2011) Sorting of an integral outer membrane protein via the lipoprotein-specific Lol pathway and a dedicated lipoprotein pilotin. *Molecular Microbiology*, 80, 655–665.

Collin, S., Krehenbrink, M., Guilvout, I. & Pugsley, A.P. (2013) The targeting, docking and anti-proteolysis functions of the secretin chaperone PulS. *Research in Microbiology*, 164, 390–396.

Collins, J., Robinson, C., Danhof, H., Knetsch, C.W., Van Leeuwen, H.C., Lawley, T.D. et al. (2018) Dietary trehalose enhances virulence of epidemic *Clostridium difficile*. *Nature*, 553, 291–294.

Cornelis, G.R. (1993) Role of the transcription activator VirF and the histone-like protein YmoA in the thermoregulation of virulence functions in Yersiniae. *Zentralblatt für Bakteriologie*, 278, 149–164.

Cornelis, G.R. (2006) The type III secretion injectisome. *Nature Reviews. Microbiology*, 4, 811–825.

Cornelis, G.R., Sluiters, C., Delor, I., Geib, D., Kaniga, K., de Rouvroit, C.L. et al. (1991) ymoA, a *Yersinia enterocolitica* chromosomal gene modulating the expression of virulence functions. *Molecular Microbiology*, 5, 1023–1034.

Cox, J. & Mann, M. (2008) MaxQuant enables high peptide identification rates, individualized p.p.b.-range mass accuracies and proteome-wide protein quantification. *Nature Biotechnology*, 26, 1367–1372.

Crago, A. & Koronakis, V. (1998) Salmonella InvG forms a ring-like multimer that requires the InvH lipoprotein for outer membrane localization. *Molecular Microbiology*, 30, 47–56.

Daefler, S. & Russel, M. (1998) The *Salmonella typhimurium* InvH protein is an outer membrane lipoprotein required for the proper localization of InvG. *Molecular Microbiology*, 28, 1367–1380.

Day, J.B. & Plano, G.V. (1998) A complex composed of SycN and YscB functions as a specific chaperone for YopN in *Yersinia pestis*. *Molecular Microbiology*, 30, 777–788.

Diepold, A., Amstutz, M., Abel, S., Sorg, I., Jenal, U. & Cornelis, G.R. (2010) Deciphering the assembly of the Yersinia type III secretion injectisome. *The EMBO Journal*, 29, 1928–1940.

Diepold, A. & Armitage, J.P. (2015) Type III secretion systems: the bacterial flagellum and the injectisome. *Philosophical Transactions of the Royal Society B: Biological Sciences*, 370, 20150020.

Diepold, A., Kudryashev, M., Delalez, N.J., Berry, R.M. & Armitage, J.P. (2015) Composition, formation, and regulation of the cytosolic C-ring, a dynamic component of the type III secretion Injectisome. *PLoS Biology*, 13, e1002039.

Diepold, A., Sezgin, E., Huseyin, M., Mortimer, T., Eggeling, C. & Armitage, J.P. (2017) A dynamic and adaptive network of cytosolic interactions governs protein export by the T3SS injectisome. *Nature Communications*, 8, 15940.

Diepold, A. & Wagner, S. (2014) Assembly of the bacterial type III secretion machinery. *FEMS Microbiology Reviews*, 38, 802–822.

Diepold, A., Wiesand, U., Amstutz, M. & Cornelis, G.R. (2012) Assembly of the Yersinia injectisome: the missing pieces. *Molecular Microbiology*, 85, 878–892.

Diepold, A., Wiesand, U. & Cornelis, G.R. (2011) The assembly of the export apparatus (YscR,S,T,U,V) of the Yersinia type III secretion apparatus occurs independently of other structural components and involves the formation of an YscV oligomer. *Molecular Microbiology*, 82, 502–514.

Erhardt, M., Namba, K. & Hughes, K.T. (2010) Bacterial nanomachines: the flagellum and type III injectisome. *Cold Spring Harbor Perspectives in Biology*, 2, a000299.

Figaj, D., Czaplewska, P., Przepióra, T., Ambroziak, P., Potrykus, M. & Skorko-Glonek, J. (2020) Lon protease is important for growth under stressful conditions and pathogenicity of the phytopathogen, bacterium *Dickeya solani*. *International Journal of Molecular Sciences*, 21, 3687.

Flacht, L., Lunelli, M., Kaszuba, K., Chen, Z.A., O'Reilly, F.J., Rappsilber, J. et al. (2023) Integrative structural analysis of the type III secretion system needle complex from *Shigella flexneri*. *Protein Science*, 32, 1–15.

Fuchs, T.M., Brandt, K., Starke, M. & Rattei, T. (2011) Shotgun sequencing of *Yersinia enterocolitica* strain W22703 (biotype 2, serotype O:9): genomic evidence for oscillation between invertebrates and mammals. *BMC Genomics*, 12, 168.

Galán, J.E. & Wolf-Watz, H. (2006) Protein delivery into eukaryotic cells by type III secretion machines. *Nature*, 444, 567–573.

Glatter, T., Ludwig, C., Ahrné, E., Aebersold, R., Heck, A.J.R. & Schmidt, A. (2012) Large-scale quantitative assessment of different in-solution protein digestion protocols reveals superior cleavage efficiency of tandem Lys-C/trypsin proteolysis over trypsin digestion. *Journal of Proteome Research*, 11, 5145–5156.

Gu, S., Rehman, S., Wang, X., Shevchik, V.E. & Pickersgill, R.W. (2012) Structural and functional insights into the pilotin-secretin complex of the type II secretion system. *PLoS Pathogens*, 8, e1002531.

Gur, E. & Sauer, R.T. (2008) Recognition of misfolded proteins by Lon, a AAA+ protease. *Genes & Development*, 22, 2267–2277.

Hardie, K.R., Lory, S. & Pugsley, A.P. (1996) Insertion of an outer membrane protein in *Escherichia coli* requires a chaperone-like protein. *The EMBO Journal*, 15, 978–988.

Hoe, N. & Goguen, J.D. (1993) Temperature sensing in *Yersinia pestis*: translation of the LcrF activator protein is thermally regulated. *Journal of Bacteriology*, 175, 7901–7909.

Hong, H., Patel, D.R., Tamm, L.K. & van den Berg, B. (2006) The outer membrane protein OmpW forms an eight-stranded β-barrel with a hydrophobic channel. *The Journal of Biological Chemistry*, 281, 7568–7577.

Hu, B., Lara-Tejero, M., Kong, Q., Galán, J.E. & Liu, J. (2017) In situ molecular architecture of the salmonella type III secretion machine. *Cell*, 168, 1065–1074.e10.

Hu, B., Morado, D.R., Margolin, W., Rohde, J.R., Arizmendi, O., Picking, W.L. et al. (2015) Visualization of the type III secretion sorting platform of *Shigella flexneri*. *Proceedings of the National Academy of Sciences of the United States of America*, 112, 1047–1052.

Hu, J., Worrall, L.J., Hong, C., Vuckovic, M., Atkinson, C.E., Caveney, N. et al. (2018) Cryo-EM analysis of the T3S injectisome reveals the structure of the needle and open secretin. *Nature Communications*, 9, 3840.

Hueck, C.J. (1998) Type III protein secretion systems in bacterial pathogens of animals and plants. *Microbiology and Molecular Biology Reviews*, 62, 379–433.

Inoue, Y., Kinoshita, M., Kida, M., Takekawa, N., Namba, K., Imada, K. et al. (2021) The FlhA linker mediates flagellar protein export switching during flagellar assembly. *Communications Biology*, 4, 646.

Iriarte, M. & Cornelis, G.R. (1999) Identification of SycN, YscX, and YscY, three new elements of the Yersinia yop virulon. *Journal of Bacteriology*, 181, 675–680.

Jackson, M.W., Silva-Herzog, E. & Plano, G.V. (2004) The ATP-dependent ClpXP and Lon proteases regulate expression of the *Yersinia pestis* type III secretion system via regulated proteolysis of YmoA, a small histone-like protein. *Molecular Microbiology*, 54, 1364–1378.

Jeckelmann, J.M. & Erni, B. (2019) *Carbohydrate transport by group translocation: the bacterial phosphoenolpyruvate: sugar phosphotransferase system*. Basel, Switzerland: Springer International Publishing.

Jeckelmann, J.M. & Erni, B. (2020) Transporters of glucose and other carbohydrates in bacteria. *Pflügers Archiv: European Journal of Physiology*, 472, 1129–1153.

Journet, L., Agrain, C., Broz, P. & Cornelis, G.R. (2003) The needle length of bacterial injectisomes is determined by a molecular ruler. *Science*, 302, 1757–1760.

Kaniga, K., Delor, I. & Cornelis, G.R. (1991) A wide-host-range suicide vector for improving reverse genetics in gram-negative bacteria: inactivation of the blaA gene of *Yersinia enterocolitica*. *Gene*, 109, 137–141.

Kinoshita, M., Hara, N., Imada, K., Namba, K. & Minamino, T. (2013) Interactions of bacterial flagellar chaperone-substrate complexes with FlhA contribute to co-ordinating assembly of the flagellar filament. *Molecular Microbiology*, 90, 1249–1261.

Kok, M., Bron, G., Erni, B. & Mukhija, S. (2003) Effect of enzyme I of the bacterial phosphoenolpyruvate: sugar phosphotransferase system (PTS) on virulence in a murine model. *Microbiology*, 149, 2645–2652.

Konovalova, A. & Silhavy, T.J. (2015) Outer membrane lipoprotein biogenesis: Lol is not the end. *Philosophical Transactions of the Royal Society B: Biological Sciences*, 370, 20150030.

Koo, J., Burrows, L.L. & Lynne Howell, P. (2012) Decoding the roles of pilotins and accessory proteins in secretin escort services. *FEMS Microbiology Letters*, 328, 1–12.

Korotkov, K.V., Gonen, T. & Hol, W.G.J. (2011) Secretins: dynamic channels for protein transport across membranes. *Trends in Biochemical Sciences*, 36(8), 433–443.

Koster, M., Bitter, W., de Cock, H., Allaoui, A., Cornelis, G.R. & Tommassen, J. (1997) The outer membrane component, YscC, of the Yop secretion machinery of *Yersinia enterocolitica* forms a ring-shaped multimeric complex. *Molecular Microbiology*, 26, 789–797.

Kudryashev, M., Diepold, A., Amstutz, M., Armitage, J.P., Stahlberg, H. & Cornelis, G.R. (2015) *Yersinia enterocolitica* type III secretion injectisomes form regularly spaced clusters, which incorporate new machines upon activation. *Molecular Microbiology*, 95, 875–884.

Kudryashev, M., Stenta, M., Schmelz, S., Amstutz, M., Wiesand, U., Castaño-Díez, D. et al. (2013) In situ structural analysis of the *Yersinia enterocolitica* injectisome. *eLife*, 2, e00792.

Kusmierek, M., Hoßmann, J., Witte, R., Opitz, W., Vollmer, I., Volk, M. et al. (2019) A bacterial secreted translocator hijacks riboregulators to control type III secretion in response to host cell contact. *PLoS Pathogens*, 15, e1007813.

Lambert de Rouvroit, C., Sluiters, C. & Cornelis, G.R. (1992) Role of the transcriptional activator, VirF, and temperature in the expression of the pYV plasmid genes of *Yersinia enterocolitica. Molecular Microbiology*, 6, 395–409.

Lampaki, D., Diepold, A. & Glatter, T. (2020) A serial sample processing strategy with improved performance for in-depth quantitative analysis of type III secretion events in *Pseudomonas aeruginosa. Journal of Proteome Research*, 19, 543–553.

Lara-Tejero, M., Kato, J., Wagner, S., Liu, X. & Galán, J.E. (2011) A sorting platform determines the order of protein secretion in bacterial type III systems. *Science*, 331, 1188–1191.

Lee, J.H., Ancona, V. & Zhao, Y. (2018) Lon protease modulates virulence traits in *Erwinia amylovora* by direct monitoring of major regulators and indirectly through the Rcs and Gac-Csr regulatory systems. *Molecular Plant Pathology*, 19, 827–840.

Majewski, D.D., Okon, M., Heinkel, F., Robb, C.S., Vuckovic, M., McIntosh, L.P. et al. (2021) Characterization of the pilotin-secretin complex from the *Salmonella enterica* type III secretion system using hybrid structural methods. *Structure*, 29, 125–138.e5.

Mazé, A., Glatter, T. & Bumann, D. (2014) The central metabolism regulator EIIAGlc switches salmonella from growth arrest to acute virulence through activation of virulence factor secretion. *Cell Reports*, 7, 1426–1433.

Miletic, S., Fahrenkamp, D., Goessweiner-Mohr, N., Wald, J., Pantel, M., Vesper, O. et al. (2021) Substrate-engaged type III secretion system structures reveal gating mechanism for unfolded protein translocation. *Nature Communications*, 12, 1546.

Milne-Davies, B., Helbig, C., Wimmi, S., Cheng, D.W.C., Paczia, N. & Diepold, A. (2019) Life after secretion—*Yersinia enterocolitica* rapidly toggles effector secretion and can resume cell division in response to changing external conditions. *Frontiers in Microbiology*, 10, 2128.

Minamino, T., Inoue, Y., Kinoshita, M. & Namba, K. (2020) FliK-driven conformational rearrangements of FlhA and FlhB are required for export switching of the flagellar protein export apparatus. *Journal of Bacteriology*, 202, e00637-1.

Miwa, H. & Okazaki, S. (2017) How effectors promote beneficial interactions. *Curr Opin Plant Biol*, 38, 148–154.

Nouwen, N., Ranson, N., Saibil, H.R., Wolpensinger, B., Engel, A., Ghazi, A. et al. (1999) Secretin PulD: association with pilot PulS, structure, and ion-conducting channel formation. *Proceedings of the National Academy of Sciences of the United States of America*, 96, 8173–8177.

Okon, M., Moraes, T.F., Lario, P.I., Creagh, A.L., Haynes, C.A., Strynadka, N.C. et al. (2008) Structural characterization of the type-III pilot-secretin complex from *Shigella flexneri. Structure*, 16, 1544–1554.

Omnus, D.J., Fink, M.J., Szwedo, K. & Jonas, K. (2021) The lon protease temporally restricts polar cell differentiation events during the caulobacter cell cycle. *eLife*, 10, 1–24.

Pacheco, A.R. & Sperandio, V. (2015) Enteric pathogens exploit the microbiota-generated nutritional environment of the gut. *Metabolism and Bacterial Pathogenesis*, 3(3), MBP-0001-2014. https://doi.org/10.1128/microbiolspec.MBP-0001-2014.

Palace, S.G., Proulx, M.K., Lu, S., Baker, R.E. & Goguen, J.D. (2014) Genome-wide mutant fitness profiling identifies nutritional requirements for optimal growth of *Yersinia pestis* in deep tissue. *MBio*, 5, e01385-14.

Perdu, C., Huber, P., Bouillot, S., Blocker, A.J., Elsen, S., Attree, I. et al. (2015) ExsB is required for correct assembly of *Pseudomonas aeruginosa* type III secretion apparatus in the bacterial membrane and full virulence in vivo. *Infection and Immunity*, 83, 1789–1798.

Pflüger-Grau, K. & Görke, B. (2010) Regulatory roles of the bacterial nitrogen-related phosphotransferase system. *Trends in Microbiology*, 18, 205–214.

Rau, R. & Darwin, A.J. (2015) Identification of YsaP, the pilotin of the *Yersinia enterocolitica* Ysa type III secretion system. *Journal of Bacteriology*, 197, 2770–2779.

Renault, T.T., Guse, A. & Erhardt, M. (2019) Export mechanisms and energy transduction in type-III secretion machines. In: *Current topics in microbiology and immunology*. Berlin, Heidelberg: Springer, pp. 1–17.

Sasakawa, C., Kamata, K., Sakai, T., Murayama, S.Y., Makino, S. & Yoshikawa, M. (1986) Molecular alteration of the 140-megadalton plasmid associated with loss of virulence and Congo red binding activity in *Shigella flexneri. Infection and Immunity*, 51, 470–475.

Schindelin, J., Arganda-Carreras, I., Frise, E., Kaynig, V., Longair, M., Pietzsch, T. et al. (2012) Fiji: an open-source platform for biological-image analysis. *Nature Methods*, 9, 676–682.

Schuch, R. & Maurelli, A.T. (1999) The mxi-Spa type III secretory pathway of *Shigella flexneri* requires an outer membrane lipoprotein, MxiM, for invasin translocation. *Infection and Immunity*, 67, 1982–1991.

Schuch, R. & Maurelli, A.T. (2001) MxiM and MxiJ, base elements of the mxi-Spa type III secretion system of Shigella, interact with and stabilize the MxiD secretin in the cell envelope. *Journal of Bacteriology*, 183, 6991–6998.

Schwiesow, L., Lam, H., Dersch, P. & Auerbuch, V. (2016) Yersinia type III secretion system master regulator LcrF. *Journal of Bacteriology*, 198, 604–614.

Silva, Y.R.d.O., Contreras-Martel, C., Macheboeuf, P. & Dessen, A. (2020) Bacterial secretins: mechanisms of assembly and membrane targeting. *Protein Science*, 29, 893–904.

Sorg, I., Wagner, S., Amstutz, M., Müller, S.A., Broz, P., Lussi, Y. et al. (2007) YscU recognizes translocators as export substrates of the Yersinia injectisome. *The EMBO Journal*, 26, 3015–3024.

Spahn, C., Laine, R.F., Pereira, P. & Gómez-de-mariscal, E. (2021) Supplementary information—DeepBacs: bacterial image analysis using open-source deep learning approaches. *bioRxiv*, 1–15.

Sturm, A., Heinemann, M., Arnoldini, M., Benecke, A., Ackermann, M., Benz, M. et al. (2011) The cost of virulence: retarded growth of Salmonella Typhimurium cells expressing type III secretion system 1. *PLoS Pathogens*, 7, e1002143.

Thevenaz, P., Ruttimann, U.E. & Unser, M. (1998) A pyramid approach to subpixel registration based on intensity. *IEEE Transactions on Image Processing*, 7, 27–41.

Troisfontaines, P. & Cornelis, G.R. (2005) Type III secretion: more systems than you think. *Physiology*, 20, 326–339.

Tseytin, I., Dagan, A., Oren, S. & Sal-Man, N. (2017) The role of EscD in supporting EscC polymerization in the type III secretion system of enteropathogenic *Escherichia coli*. *Biochimica et Biophysica Acta*, 1860, 384–395.

Tsilibaris, V., Maenhaut-Michel, G. & Van Melderen, L. (2006) Biological roles of the Lon ATP-dependent protease. *Research in Microbiology*, 157, 701–713.

Tyanova, S., Temu, T., Sinitcyn, P., Carlson, A., Hein, M.Y., Geiger, T. et al. (2016) The Perseus computational platform for comprehensive analysis of (prote)omics data. *Nature Methods*, 13, 731–740.

Wagner, S. & Diepold, A. (2020) A unified nomenclature for injectisome-type type III secretion systems. *Current Topics in Microbiology and Immunology*, 427, 1–10.

Wagner, S., Grin, I., Malmsheimer, S., Singh, N., Torres-Vargas, C.E. & Westerhausen, S. (2018) Bacterial type III secretion systems: a complex device for the delivery of bacterial effector proteins into eukaryotic host cells. *FEMS Microbiology Letters*, 365, fny201.

Wallace, I.M., O'Sullivan, O., Higgins, D.G. & Notredame, C. (2006) M-Coffee: combining multiple sequence alignment methods with T-Coffee. *Nucleic Acids Research*, 34, 1692–1699.

Wang, Q., Millet, Y.A., Chao, M.C., Sasabe, J., Davis, B.M. & Waldor, M.K. (2015) A genome-wide screen reveals that the Vibrio cholerae phosphoenolpyruvate phosphotransferase system modulates virulence gene expression. *Infection and Immunity*, 83, 3381–3395.

Wee, D.H. & Hughes, K.T. (2015) Molecular ruler determines needle length for the *Salmonella* Spi-1 injectisome. *Proceedings of the National Academy of Sciences of the United States of America*, 112, 4098–4103.

Wimmi, S., Balinovic, A., Jeckel, H., Selinger, L., Lampaki, D., Eisemann, E. et al. (2021) Dynamic relocalization of cytosolic type III secretion system components prevents premature protein secretion at low external pH. *Nature Communications*, 12, 1625.

Wu, X.-B., Tian, L.-H., Zou, H.-J., Wang, C.-Y., Yu, Z.-Q., Tang, C.-H. et al. (2013) Outer membrane protein OmpW of *Escherichia coli* is required for resistance to phagocytosis. *Research in Microbiology*, 164, 848–855.

Xing, Q., Shi, K., Portaliou, A.G., Rossi, P., Economou, A. & Kalodimos, C.G. (2018) Structures of chaperone-substrate complexes docked onto the export gate in a type III secretion system. *Nature Communications*, 9, 1773.

Yin, M., Yan, Z. & Li, X. (2018) Structural insight into the assembly of the type II secretion system pilotin–secretin complex from enterotoxigenic *Escherichia coli*. *Nature Microbiology*, 3, 581–587.

Zhang, Y., Lara-Tejero, M., Bewersdorf, J. & Galán, J.E. (2017) Visualization and characterization of individual type III protein secretion machines in live bacteria. *Proceedings of the National Academy of Sciences of the United States of America*, 114, 6098–6103.

Zhou, X., Teper, D., Andrade, M.O., Zhang, T., Chen, S., Song, W.Y. et al. (2018) A phosphorylation switch on lon protease regulates bacterial type III secretion system in host. *MBio*, 9, e02146-17.

SUPPORTING INFORMATION

Additional supporting information can be found online in the Supporting Information section at the end of this article.